Article

Brown Adipose Tissue and Skeletal Muscle Coordinately Contribute to Thermogenesis in Mice

Yuna Izumi-Mishima,[1] Rie Tsutsumi,[1] Tetsuya Shiuchi,[2] Saori Fujimoto,[1] Momoka Taniguchi,[1] Yuko Okamatsu-Ogura,[3] Takeshi Yoneshiro,[4] Masashi Kuroda,[1] Kazuhiro Nomura,[1] and Hiroshi Sakaue[1,5,*]

[1]Department of Nutrition and Metabolism, Institute of Biomedical Sciences, Tokushima University Graduate School, Tokushima 770-8503, Japan
[2]Department of Integrative Physiology, Institute of Biomedical Sciences, Tokushima University Graduate School, Tokushima 770-8503, Japan
[3]Laboratory of Biochemistry, Faculty of Veterinary Medicine, Hokkaido University, Sapporo 060-0818, Japan
[4]Division of Molecular Physiology and Metabolism, Tohoku University Graduate School of Medicine, Sendai 980-8575, Japan
[5]Lead contact
*Correspondence: hsakaue@tokushima-u.ac.jp

Abstract

Endotherms increase the rate of metabolism in metabolic organs as one strategy to cope with a decline in temperature of the external environment. However, an additional major contributor to maintenance of body temperature in a cold environment is contraction-based thermogenesis in skeletal muscle. Here we show that impairment of hind limb muscle contraction by cast immobilization suppresses skeletal muscle thermogenesis and activates brown adipose tissue (BAT) thermogenesis as a compensatory mechanism. BAT utilizes free branched-chain amino acids (BCAAs) derived from skeletal muscle as an energy substrate for thermogenesis, and interleukin-6 released by skeletal muscle stimulates BCAA production in muscle for support of BAT thermogenesis. Our findings suggest that BAT and skeletal muscle cooperate to maintain body temperature in endotherms.

Introduction

Endotherms rely on the regulation of heat generation by metabolism in tissues of the body to maintain a stable core body temperature in the face of a fluctuating temperature of the external environment and thereby to ensure optimal physiological function.[1] Small mammals adjust their metabolic rate to cope with temperature fluctuations and to support their survival during seasonal acclimation. Some mammalian species are able to lower their metabolic rate and enter a state of torpor or hibernation in order to conserve energy and ensure survival.[2] However, small mammals that do not hibernate must increase their rate of metabolism, including obligatory thermogenesis in metabolic organs such as the liver and skeletal muscle as well as regulatory thermogenesis (shivering or nonshivering thermogenesis) in skeletal muscle and brown adipose tissue (BAT), in order to maintain thermal homeostasis in a cold environment.[1,3,4]

Under normothermic conditions, core body temperature is determined by basal metabolic organs such as the brain, heart, liver, and skeletal muscle. [1] Skeletal muscle is the largest weight-bearing organ in humans and consumes a substantial amount of energy, even at rest. Shivering is the major source of heat production in acute cold exposure before sufficient amount of UCP1 (uncoupling protein 1) can be recruited in BAT[1,5,6]. Shivering is gradually replaced by UCP1 dependent thermogenesis and nonshivering thermogenesis is necessary for long-term adaptation to a cold environment. [5] Skeletal muscle and BAT thermogenesis can compensate in part each other to maintain core body temperature is widely recognaized[5-8], and recent study suggests that suppression of BAT thermogenesis has been found to promote thermogenesis in skeletal muscle.[8]

While skeletal muscle is the critical metabolic organ, it also stores an abundance of amino acids as energy substrates in the form of muscle proteins.[9] Skeletal muscle also has the plasticity for adapting to environmental conditions and shows metabolic flexibility in response to the substrate requirements of other organs and thereby contributes to the maintenance of energy balance.[9,10] Activation of BAT themogenesis is associated with increased lipid and glucose catabolism.[11-13] Succinate and branched-chain amino acids (BCAAs) have also been found to support BAT thermogenesis, however.[14–16] Although succinate may be provided by muscle contraction,[14,17] the primary source of BCAAs for BAT thermogenesis has remained unclear. Indeed, mitochondrial BCAA

catabolism in brown adipocytes promotes systemic BCAA clearance. Skeletal muscle may therefore also respond to the energy demands of BAT.

Whereas body temperature and energy metabolism in metabolic organs are closely related, how they are regulated in a coordinated manner is poorly understood. Several endocrine factors alter metabolism in abdominal organs.[18] In particular, interleukin (IL)–6 is an endocrine factor that plays multiple roles in the response of the body to infection, exercise, and stress as well as in inflammation.[19–21] IL-6 induces various fever responses, including nonshivering thermogenesis in BAT, by promoting prostaglandin E2 (PGE2) synthesis in central vascular endothelial cells.[22] On the other hand, IL-6 directly affects energy metabolism in various organs, including skeletal muscle, liver, and adipose tissue.[23–27] These multiple roles suggest that IL-6 is a key molecule linking thermogenesis and energy metabolism.

Here we show that suppression of skeletal muscle thermogenesis by cast immobilization in mice activates a compensatory thermoregulatory system dependent on BAT thermogenesis. We also show that free BCAAs derived from skeletal muscle support BAT thermogenesis, and we identify IL-6 as a key regulator of this system. Our findings reveal the importance of skeletal muscle as a source of amino acids and uncover a previously unrecognized thermoregulatory system mediated by BAT and skeletal muscle metabolism.

Results

Cast immobilization suppresses muscle thermogenesis and activates a compensatory thermoregulatory system

We first examined the role of skeletal muscle in endothermic homeostasis by performing an acute cold tolerance test at 4°C for 4 h in mice with both hind limbs immobilized in casts. We confirmed that ~50% of systemic skeletal muscle was immobilized (Table S1), and that the immobilization induced skeletal muscle atrophy within 3 to 5 days (Figure 1_figure supplement 1A–1C). Consistent with previous findings,[28] we found that gene expression for the ubiquitin ligases Atrogin-1 and MuRF-1 was increased during the early phase (days 1–3) of cast immobilization (Figure 1_figure supplement 1D and 1E). We also found that expression of the *Ppargc1a* (PGC-1α), a master regulator of mitochondrial biogenesis and oxidative metabolism, was decreased from 10 h after cast immobilization and the amount of *Tfam* (transcription factor A, mitochondrial) mRNA was subsequently decreased in immobilized muscle

109 (Figure 1_figure supplement 1F and 1G). Metabolomic profiling of the
110 immobilized muscle revealed decreases in the amounts of fumaric acid and
111 malic acid within 1 day of cast immobilization (Figure 1_fugure supplement 1H).
112 Mice with both hind limbs immobilized for 7 days showed a significantly lower
113 core body temperature after cold exposure compared with control mice (Figure
114 1A). Cast immobilization for 24 h also induced cold intolerance with
115 preservation of muscle mass (Figure 1B and Figure 1_figure supplement 1A-
116 1C). To investigate whether cold intolerance depends on the immobilized
117 muscle mass, we examined the change in core body temperature in mice with
118 unilateral immobilization. Systemic locomotor activity during cold exposure was
119 similar for mice with unilateral or bilateral immobilization and for control mice
120 (Figure 1_figure supplement 1I). However, the decrease in body temperature
121 induced by cold exposure in mice with unilateral immobilization was attenuated
122 compared with that in mice subjected to bilateral immobilization (Figure 1C).
123 These findings suggested that immobilization of skeletal muscle suppresses
124 thermogenesis in this organ and it may negatively affects the maintenance of
125 body temperature under cold environments independently of locomotor activity.
126 Mice subjected to cast immobilization showed cold intolerance (Figure 1A
127 and B), but the core body temperature of cast-immobilized mice and control
128 mice were little different under room temperature (Figure 1D). We then
129 examined the effects of such immobilization on interscapular BAT (iBAT) to
130 investigate the mechanism underlying the maintenance of core body
131 temperature in mice with cast immobilization. Expression of UCP1 at the mRNA
132 and protein levels as well as the abundance of PGC-1α, a transcriptional
133 cofactor that promotes the expression of thermogenesis-related genes, showed
134 transient increases in iBAT after cast immobilization (Figures 1E–1H).
135 Expression of *Ucp1* mRNA in iBAT was significantly increased after cold
136 exposure compared to control mice at room temperature, whereas those
137 expression were not induced by cole exposure in cast immobilized mice (Figure
138 1_figure supplement 1J). Small and multilocular lipid droplets were apparent in
139 adipocytes of iBAT within 24 h of cast immobilization (Figure 1_figure
140 supplement 1K). However, mice subjected to cast immobilization showed no
141 increase in food consumption or activity levels (Figure 1_figure supplement 1L–
142 1N). These results indicated that the suppression of muscle thermogenesis by
143 cast immobilization induces BAT thermogenesis without an increase in food
144 consumption or activity levels. On the other hand, the amount of *Sln* (sarcolipin)
145 and *Camk2a* (Ca^{2+}- and calmodulin-dependent protein kinase II) mRNA were

146 not affected in immobilized muscle (Figure 1_figure supplement 1O and 1P).
147 These findings thus suggested that nonshivering thermogenesis was induced
148 minimally in cast-immobilized skeletal muscle. Cast immobilization thus
149 preferentially activated nonshivering thermogenesis in BAT, not in skeletal
150 muscle.
151
152 **Cast immobilization promotes BAT thermogenesis via sympathetic**
153 **activation**
154 We next explored the mechanism underlying the activation of BAT
155 thermogenesis by cast immobilization. We first focused on the sympathetic
156 nervous system, a general inducer of BAT thermogenesis,[29] and found that the
157 norepinephrine concentration in iBAT was tended to increased after 24 h of cast
158 immobilization (Figure 1I). We then subjected mice to sympathetic denervation
159 of iBAT. Expression of *Ucp1* mRNA in iBAT was significantly attenuated by such
160 denervation in mice with or without subsequent cast immobilization (Figure 1J).
161 Whereas adipocytes of iBAT showed small and multilocular lipid droplets after 7
162 days of cast immobilization in sham-operated mice, iBAT of mice subjected to
163 surgical denervation was hypertrophied and did not show such lipid droplets
164 (Figure 2_figure supplement 2A). Moreover, mice with denervated iBAT
165 manifested a lower core body temperature compared with sham-operated mice
166 after cold exposure at 4°C for 1 h, and cast immobilization further increased the
167 extent of hypothermia in the denervated mice (Figure 1K). These results
168 suggested that BAT thermogenesis is activated via sympathetic nerves to
169 maintain core body temperature in cast-immobilized mice.
170
171 **Cast immobilization alters systemic metabolic dynamics associated with**
172 **BAT thermogenesis**
173 We next examined the metabolic dynamics of iBAT as well as systemic
174 metabolic changes in mice subjected to cast immobilization. Metabolomics
175 analysis revealed increases in the amounts of carbohydrate metabolites and
176 amino acids in iBAT that were apparent as early as 24 h after cast
177 immobilization, and that such increases were not apparent in mice with iBAT
178 denervation (Figures 2A and 2B). Brown adipocytes incorporate fatty acids and
179 various other energy substrates to initiate thermogenesis and contribute to the
180 maintenance of core body temperature.[30] We found that expression of the
181 genes for fatty acid (Figure 2C) and succinate (Figure 2D) transporters in iBAT

was induced by cast immobilization and that such induction was prevented by iBAT denervation. The concentration of succinate was also increased in iBAT of cast-immobilized mice in a manner sensitive to iBAT denervation (Figure 2E). Consistent with these changes in metabolite levels, oxygen consumption and systemic lipid utilization were increased by cast immobilization in intact mice (Figures 2F and 2G) but not in those subjected to iBAT denervation (Figure supplement 1A and 1B).

The weight of epididymal white adipose tissue (eWAT) and hepatic glycogen content were reduced by cast immobilization (Figures 2H and 2I). Expression of the genes for glucose-6-phosphatase (G6Pase) and phosphoenolpyruvate carboxykinase (PEPCK) in the liver increased gradually after cast immobilization, peaking at day 5 (Figure 2_figure supplement 1C and 1D), suggesting that gluconeogenesis was slowly activated in the cast-immobilized mice. Metabolomic profiling of the liver revealed marked increases in the amounts of 3-phosphoglyceric acid and 2-phosphoglyceric acid within 1 day of cast immobilization (Figure 2_figure supplement 1E), suggesting that glycerol influx was also enhanced in the liver. Together, these results thus indicated that cast immobilization affects metabolic dynamics in the liver and WAT, and that these changes might occur after the activation of BAT thermogenesis.

The serum concentration of norepinephrine was increased within 1 day of cast immobilization (Figure 2_figure supplement 1F), but these metabolic changes induced by cast immobilization were not associated with by an increase in the serum concentration of corticosterone or in expression of the gene for corticotropin-releasing hormone (CRH) in the hypothalamus (Figure 2_figure supplement 1G and 1H). These results suggest that cast immobilization may activates BAT thermogenesis and systemic metabolic changes through lower body temperature resulting from suppression of muscle thermogenesis rather than stress.

Free amino acids are transferred from skeletal muscle to BAT and the liver for energy homeostasis

We next focused on metabolism of amino acids in BAT and skeletal muscle in mice after cast immobilization. As shown above, amino acid concentrations in iBAT were increased by cast immobilization in a manner sensitive to denervation of iBAT (Figure 2B). The amounts of free amino acids were also

increased in both soleus and extensor digitorum longus (EDL) muscles of cast-immobilized mice (Figure 3A), whereas those in serum and the liver were not increased by cast immobilization (Figure 3B). We then examined gene expression profiles for solute carrier (SLC) transporters that mediate the transport of amino acids across cell membranes as well as for mitochondrial BCAA catabolic enzymes (BCAT2, branched-chain aminotransferase 2; BCKDHA, branched-chain keto acid dehydrogenase E1 subunit α) in iBAT, liver, and soleus. The expression of these genes in iBAT was increased after cast immobilization for 10 to 24 h, whereas that in the liver was increased after 5 to 7 days (Figure 3C). In particular, expression of the genes for SLC1A5 (a sodium-dependent glutamate transporter) and SLC38A2 (a sodium-coupled neutral amino acid transporter) was significantly increased in iBAT after cast immobilization for 10 h (Figure 3_figure supplement 1A–1F). In the liver, expression of the gene for SLC38A2, which is upregulated by extracellular amino acid deprivation,[31,32] and of that for BCKDHA, which is thought to be upregulated under fasting conditions to oxidize BCAAs for gluconeogenesis,[33,34] was significantly increased by cast immobilization (Figure 3C and Figure3_figure supplement 1G–1K). On the other hand, gene expression for amino acid transporters (SLC1A5, SLC7A5, SLC38A2) and BCAA catabolic enzymes (BCAT2, BCKDHA) in soleus was significantly decreased after cast immobilization (Figure 3C and Figure 3_figure supplement 1L–1Q). Expression of the gene for SLC43A1, which is upregulated by food deprivation and is thought to transport amino acids from cells to the external environment,[35] was significantly increased in soleus by cast immobilization (Figure 3C and Figure 3_figure supplement 1O).

We next investigated amino acid incorporation in tissues by administration of [^{3}H]leucine into the tail vein of mice. Incorporation of [^{3}H]leucine was not increased in skeletal muscle of mice subjected to cast immobilization for 1 or 3 days (data not shown), whereas it was significantly increased in iBAT, liver, and kidney of those subjected to cast immobilization for 1 day (Figure 3D). Gene expression for SLC25A44, a mitochondrial BCAA transporter that contributes to BAT thermogenesis,[15] was increased in iBAT at 24 h after cast immobilization (Figure 3E and Figure 3_figure supplement 1R–1T). However, the early increases in expression of the genes for SLC25A44, SLC1A5, and SLC38A2 induced by cast immobilization in iBAT of intact mice were prevented by denervation of iBAT (Figure 3E and Figure 3_figure

254 supplement 1U–1AA). Our results thus suggested that free amino acids are
255 utilized as an energy substrate in BAT and the liver rather than in skeletal
256 muscle of cast-immobilized mice.
257
258 **Cast immobilization upregulates IL-6 gene expression in BAT and skeletal**
259 **muscle**
260 We next set out to identify regulatory molecules that might contribute to the
261 maintenance of body temperature and to the systemic metabolic changes in
262 cast-immobilized mice. Gene expression analysis revealed that the IL-6 gene
263 tended to be induced earlier and to a greater extent in iBAT and soleus than
264 were genes for other cytokines including tumor necrosis factor–α (TNF-α),
265 monocyte chemoattractant protein–1 (MCP-1), IL-1β, IL-10, and IL-15; for
266 batokines including fibroblast growth factor 21 (FGF21) and bone
267 morphogenetic protein 8B (BMP8B); or for myokines including FGF21 and irisin
268 (Figures 4A–4D and Figure 4_figure supplement 1A–1N). Whereas the increase
269 in the amount of *Il6* mRNA was apparent as early as 6 to 10 h in iBAT, that in
270 soleus was more gradual (Figures 4C and 4D). IL-6 has been found to be
271 released by various organs, including adipose tissue and skeletal muscle, in
272 response to inflammation, stress, or exercise.[18-21] The abundance of *Il6* mRNA
273 in liver, eWAT, or spleen was not affected by cast immobilization (Figure
274 4_figure supplement 1O–1Q). Expression of the genes for serum amyloid A3
275 (*Saa3*) and suppressor of cytokine signaling 3 (*Socs3*), both of which are
276 regulated by IL-6 signaling, was also increased in iBAT and soleus at the same
277 time as was that of *Il6* (Figures 4E–4H). Expression of these genes was also
278 increased in the liver or eWAT at 10 or 24 h after cast immobilization (Figures
279 4I–4L). However, expression of *Il6* was not induced by cast immobilization in
280 denervated iBAT (Figures 4M). The serum concentration of IL-6 was
281 significantly increased from 10 h after cast immobilization (Figure 4N), whereas
282 that of TNF-α was not altered in cast-immobilized mice (Figure 4_figure
283 supplement 1R). Together, these results suggested that cast immobilization
284 induces *Il6* expression in iBAT and skeletal muscle, and that induction of *Il6*
285 expression by cast immobilization in iBAT is dependent on the sympathetic
286 nervous system.
287
288 **IL-6 affects energy metabolism in BAT and skeletal muscle of cast-**
289 **immobilized mice**
290 We investigated the role of IL-6 in the skeletal muscle–BAT
291 thermoregulatory system with the use of subjected IL-6 knockout (KO) mice to

292 cast immobilization. Expression of *Ucp1* in iBAT was significantly increased at
293 24 h after cast immobilization in both WT and IL-6 KO mice (Figure 5_figure
294 supplement 1A). However, core body temperature of cast-immobilized IL-6 KO
295 mice was decreased to a greater extent by cold exposure at 4°C for 4 h
296 compared with that of cast-immobilized WT mice (Figure 5A). Furthermore,
297 unlike that in WT mice, oxygen consumption was not increased in IL-6 KO mice
298 after cast immobilization (Figure 5_figure supplement 1B and 1C).
299 Metabolomics analysis revealed that the amounts of carbohydrate metabolites
300 including glucose 1-phosphate, glucose 6-phosphate, and phosphoenolpyruvic
301 acid in iBAT were higher for IL-6 KO mice than for WT mice, and were not
302 increased substantially by cast immobilization in the mutant mice (Figure 5B).
303 Whereas the concentrations of amino acids such as Ser, Asn, Lys, Met, His,
304 Phe, and Tyr in iBAT of WT mice were increased markedly at 24 h after cast
305 immobilization, such was not the case for IL-6 KO mice (Figure 5C). Expression
306 of the genes for SLC25A44, BCKDHA, and CD36 in iBAT was higher for IL-6
307 KO mice than for WT mice, but expression of the genes for SLC25A44 and
308 CD36 in iBAT of IL-6 KO mice was not increased further at 24 h after cast
309 immobilization (Figures 5D–5F). Incorporation of [^{3}H]leucine was also not
310 increased in iBAT of IL-6 KO mice after cast immobilization for 24 h (Figure 5G).
311 In addition, adipocytes with small and multilocular lipid droplets were observed
312 in iBAT of IL-6 KO mice with or without cast immobilization (Figure 5_figure
313 supplement 1D). The respiratory exchange ratio (RER) of WT mice was
314 significantly decreased in both the light and dark phases for the first 5 days of
315 cast immobilization, whereas similar differences were apparent only for the first
316 2 days in IL-6 KO mice (Figure 5_figure supplement 1E and 1F). IL-6 has been
317 shown to promote lipolysis and fatty acid oxidation in WAT.[26] We found that,
318 unlike in WT mice, cast immobilization did not result in a loss of eWAT mass in
319 IL-6 KO mice (Figure 5_figure supplement 1G). Collectively, these data
320 suggested that utilization of energy substrates was not substantially altered by
321 cast immobilization in IL-6 KO mice.
322 The amounts of BCAAs in soleus were significantly increased after cast
323 immobilization in WT mice but not in IL-6 KO mice (Figures 5H–5J). Serum
324 BCAA concentrations were decreased after cast immobilization in both WT and
325 IL-6 KO mice (Figure 5_figure supplement 1H–1J). These findings suggested
326 that deficiency of IL-6 impairs the maintenance of core body temperature and
327 alters energy metabolism in BAT and skeletal muscle in mice subjected to cast
328 immobilization.
329

330 **Administration of IL-6 increases BCAA concentrations in skeletal muscle**
331 **of cast-immobilized IL-6 KO mice**
332 We examined whether administration of exogenous IL-6 might increase amino
333 acid concentrations in skeletal muscle and BAT of IL-6 KO mice with cast
334 immobilization. Administration of IL-6 restored the increase in the amounts of
335 amino acids including BCAAs in soleus of IL-6 KO mice with cast immobilization
336 (Figures 6A–6C and Figure 6_figure supplement 1A). Treatment with IL-6 also
337 increased expression of *Saa3* and *Socs3* (Figure 6_figure supplement 1B and
338 1C) as well as the amounts of BCAAs (Figure 6D) in cultured mouse C2C12
339 myotubes. However, the amounts of carbohydrate metabolites in iBAT of cast-
340 immobilized IL-6 KO mice were not increased by IL-6 administration (Figure
341 6_figure supplement 1D). In contrast to its effects on soleus, administration of
342 IL-6 also did not increase the amounts of amino acids in iBAT of IL-6 KO mice
343 with cast immobilization (Figure 6_figure supplement 1A and 1E). In addition,
344 exogenous IL-6 did not increase the expression of UCP1, SLC25A44, and
345 BCKDHA genes in iBAT of these mice (Figure 6_figure supplement 1F–1H). On
346 the other hand, administration of IL-6 ameliorated the cold intolerance of IL-6
347 KO mice with cast immobilization (Figure 6E). We therefore examined whether
348 IL-6 might increase core body temperature via the sympathetic nervous system
349 with the use of C57BL/6J mice with denervated iBAT. Core body temperature of
350 cold-exposed mice with cast immobilization and denervated iBAT was not
351 significantly increased by administration of IL-6 (Figure 6F).
352 We also found that the core body temperature of IL-6 KO mice was lower
353 than that of WT mice after cold exposure at 4°C for 4 h (Figure 6_figure
354 supplement 1I) whereas the amount of *Ucp1* mRNA in iBAT was significantly
355 increased for IL-6 KO mice compared with WT mice at room temperature
356 (Figure 6_figure supplement 1J). We then investigated the possible direct
357 effects of IL-6 on energy metabolism in BAT with the use of cultured mouse
358 brown adipocytes. Expression of the SLC25A44, BCKDHA, and UCP1 genes in
359 the brown adipocytes were not increased by treatment with IL-6 (Figure 6_figure
360 supplement 1K–1M). In contrast, treatment with the β_3-adrenergic receptor
361 agonist CL316 243 increased the expression of these genes, and this
362 upregulation was suppressed by treatment with IL-6 (Figure 6_figure
363 supplement 1K–1M). Long-term administration of CL316 243 in mice was
364 previously shown to increase expression of *Ucp1*, *Slc25a44*, and *Bckdha* in
365 BAT.[16] We found that administration of CL316 243 for 7 days significantly
366 increased the amounts of *Ucp1*, *Slc25a44*, and *Bckdha* mRNAs in iBAT of IL-6

KO mice but not in that of WT mice (Figure 6_figure supplement 1N–1P). Together, these data suggested that IL-6 may suppress β-adrenergic receptor–mediated thermogenesis and BCAA metabolism in brown adipocytes. Nevertheless, IL-6 induces fever response through stimulation of the central[21,22] and uptake of energy-rich BCAA delivered to BAT from skeletal muscle may facilitate a net induction of BAT thermogenesis.

Skeletal muscle–derived IL-6 increases BCAA concentrations in skeletal muscle for BAT thermogenesis

Given that our data suggested that an elevated blood concentration of IL-6 contributes to maintenance of body temperature in cast-immobilized mice in a manner dependent on the sympathetic nervous system (Figures 6E and 6F), we sought to determine the main source of circulating IL-6 in cast-immobilized mice. We first focused on the acute expression of the IL-6 gene apparent in iBAT after cast immobilization (Figure 4C), and we subjected mice to surgical removal of iBAT. The serum IL-6 concentration of such mice was not increased after cast immobilization (Figure 6G). We also found that the reduction in eWAT mass after cast immobilization in C57BL/6J mice was suppressed by surgical removal of iBAT (Figure 6H). These results suggested that BAT-derived IL-6 induces lipolysis in WAT.

We further investigated the effects of BAT-derived IL-6 on skeletal muscle. Whereas the serum concentration of IL-6 in mice depleted of iBAT was not affected by cast immobilization (Figure 6G), the concentrations of BCAAs in soleus were increased after cast immobilization in such mice (Figures 6I–6K). The amount of *Slc43a1* mRNA in soleus of mice depleted of iBAT was significantly increased by cast immobilization (Figure 6_figure supplement 2A). Gene expression for other amino acid transporters (such as SLC1A5 and SLC7A5) and for BCAA catabolic enzymes (BCAT2 and BCKDHA) in soleus also showed a similar pattern of changes after cast immobilization in iBAT-depleted mice (Figure 6_figure supplement 2B–2E) as in intact mice (Figure 3_figure supplement Fig. 1L, 1M, 1P, and 1Q). Moreover, cast immobilization for 7 days induced similar losses of both soleus and gastrocnemius mass in mice with or without removal of iBAT (Figure 6_figure supplement 2F and Table S2). These data thus suggested that IL-6 secretion in an autocrine or paracrine manner may regulate BCAA metabolism in skeletal muscle independently of IL-6 derived from iBAT.

Acute cold exposure also induced IL-6 from skeletal muscle to supply BCAA for BAT thermogenesis

We further found that expression of *Il6* was also increased in not immobilized fore limb muscles (biceps brachii muscle; BBM) after cast immobilization (Figure 6_figure supplement 2G). Expression of *Saa3* and *Socs3* were increased in BBM at the same time as was that of *Il6* after cast immobilization (Figure 6_figure supplement 2H and 1I). Furthermore, gene expression for the ubiquitin ligases Atrogin-1 and MuRF-1 in BBM was increased during the early phase of cast immobilization (Figure 6_figure supplement 2J and 2K). BCAA concentrations in BBM were also increased after cast immobilization (Figure 6_figure supplement 2L-2N). These data suggest that cast immonbilization stimulates BCAA metabolits in not immobilized fore limb muscles as well as immobilized muscle.

Finally, we investigated whether the thermoregulatory system through amino acid metabolism in the interaction between BAT and skeletal muscle also plays an important role in other conditions besides cast immobilization. Acute cold exposure also increased expression of *Il6* only in iBAT and skeletal muscle in mice (Figure 6L). Expression of *Saa3* and *Socs3* were increased in soleus (Figures 6M and 6N), and both soleus and gastrocnemius mass were decreased by cold exposure at 4°C for 4 h (Figure 6_figure supplement 2O and 2P). Furthermore, the amounts of valine in soleus were significantly increased by acute cold exposure in WT mice but not in IL-6 KO mice (Figures 6O and 6P). BCAA concentrations in soleus were also increased after cold exposure at 4°C for 4 h in iBAT-depleted mice (Figure 6_figure supplement 2Q). Together, thermoregulatory system through amino acid metabolism in skeletal muscle and BAT may be activated via sympathetic nervous system under cold temperature.

Discussion

We have here shown that cast immobilization suppressed skeletal muscle thermogenesis, resulting in failure to maintain core body temperature in a cold environment. Cast immobilization also activated BAT thermogenesis via the sympathetic nervous system and triggered systemic changes in energy metabolism associated with BAT thermogenesis. In addition, we found that free BCAAs derived from skeletal muscle serve as substrates for energy metabolism in BAT, and that skeletal muscle–derived IL-6 promotes this provision of BAT

439 with amino acids from muscle.

440 Exercise-induced muscle contraction generates large amounts of heat
441 which dependents on hydrolysis of ATP, and skeletal muscle, as the first organ
442 to be recruited for thermogenesis, plays an important role in maintenance of
443 body temperature in endotherms.[36] Muscle thermogenesis can account for up to
444 90% of systemic oxygen consumption during periods of maximal recruitment of
445 muscle contraction, such as during exercise or an intense bout of shivering.[36,37]
446 We found that cast immobilization suppressed mitochondria related genes
447 expression and metabolites of TCA cycle from early stage of immobilization,
448 suggesting that metabolic rate is rapidly decreased in immobilized muscle. Thus
449 our results of cast immobilization leading cold intolerance in mice show that
450 metabolic thermogenesis in skeletal muscle plays a key role in mammals even
451 in BAT-enriched mammals such as rodents.

452 Thermoregulatory system in endotherms cannot be explained by
453 thermogenesis based on muscle contraction alone, with nonshivering
454 thermogenesis being required as a component of the ability to tolerate cold
455 temperatures in the long term[1]. Our results now show that expression of the
456 gene for sarcolipin, a key regulator of the sarco/endoplasmic reticulum Ca^{2+}-
457 ATPase (SERCA) and an important mediator of muscle nonshivering
458 thermogenesis, was not increased in muscle after cast immobilization. On the
459 other hand, BAT thermogenesis was activated via the sympathetic nervous
460 system even when skeletal muscle was immobilized. It is a well-recognized fact
461 that BAT and skeletal muscle function in an orchestrated manner to maintain
462 core body temperature in endotherms[5-7]. A bit surprisingly, BAT capacity itself
463 was not sufficient to maintain stable body temperature under acute cold
464 exposure, whereas compensatory BAT recruitment protected cast immobilized
465 mice from hypothermia at room temperature.

466 We also found that changes in systemic energy metabolism induced by
467 cast immobilization were associated with the activation of BAT thermogenesis.
468 Activation of BAT results in the tissue becoming a high consumer of a variety of
469 energy substrates including lipids, glucose, BCAAs, succinate, and lactate.[30] In
470 addition, our results suggest that skeletal muscle is a source of free amino acids
471 for BAT thermogenesis or hepatic gluconeogenesis. In response to metabolic
472 demands imposed by starvation, exercise, or cold exposure, for example,
473 skeletal muscle manifests metabolic flexibility in order to meet the demands of
474 other organs and is an important determinant of metabolic homeostasis.[9,10] In

475 contrast, the reduction in metabolic rate may contribute to protein conservation
476 and maintain skeletal muscle mass under hibernation.[9] Our findings now
477 provide new insight into the importance of skeletal muscle as a source of amino
478 acids, with a recent study also suggesting that a highly active proteolysis
479 system in the heart provides substantial amounts of amino acids for distribution
480 to other organs via the bloodstream.[38] The heart may therefore be another
481 source of free BCAAs for BAT thermogenesis in cast-immobilized mice.
482 We found that muscle-derived IL-6 directly increased the abundance of
483 BCAAs in skeletal muscle after cast immobilization. Previous studies have
484 shown that excessive IL-6 induces amino acid catabolism in skeletal
485 muscle,[39,40] and that IL-6 is one of the factors responsible for the induction of
486 muscle atrophy in cast-immobilized mice.[41] IL-6 is a secreted factor induced by
487 several mechanisms including muscle contraction, intracellular calcium
488 signaling, and inflammation.[20,42] However, inflammation associated with
489 macrophage infiltration is not thought to be induced in the early stages of
490 muscle atrophy[28], and thus inflammation-induced IL-6 expression may therefore
491 not contribute to the changes in amino acid metabolism in cast-immobilized
492 muscle. In addition, whereas intracellular calcium concentrations may increase
493 after muscle immobilization for 2 weeks,[43] they appear to decrease in response
494 to short-term cast immobilization.[41] Cast immobilization–induced *Il6* expression
495 may therefore also not be regulated by calcium signaling. Upregulation of IL-6
496 expression by cast immobilization was previously shown to be mediated by a
497 Piezo1-KLF15 axis, [41] whereas our observation that *Il6* expression were
498 increased in non immobilized fore limb muscles. Furthermore, acute cold
499 exposure tended to increase *Il6* expression in skeletal muscle, suggesting that
500 muscle-derived IL-6 for thermoregulatory system may also be regulated by the
501 central nervous system. A recent study showed that motor circuits modulate the
502 production of neutrophil-induced chemokines in skeletal muscle after acute
503 stress.[44] The regulation of IL-6 production in muscle by the central nervous
504 system warrants further investigation.
505 The central nervous system tightly controls core body temperature
506 through integrates information about external temperature, humidity, and
507 thermal sensation to induce an adaptive response.[1] Disappointingly, our study
508 was inconclusive as to whether the trigger for BAT thermogenesis after cast
509 immobilization was hypothermia associated with supression of muscle
510 thermogenesis or stress. However, we found that acute cold exposure also

511 recruits substrate supply from skeletal muscle for BAT thermogenesis. Possibly,
512 thermoregulatory system through amino acid metabolism in skeletal muscle and
513 BAT may also be an important metabolic strategy even in the case of fever
514 responce induced by stress or infection. Furthermore, inflammation, infection,
515 and acute stress trigger rapid increases in the circulating IL-6 concentration[21,45]
516 and induce a fever response by promoting PGE2 synthesis. Mitochondrial
517 BCAA oxidation in BAT was recently shown to be increased to support
518 thermogenesis induced by PGE2.[16] We found that BAT-derived IL-6 increased
519 blood IL-6 levels after cast immobilization and administration of exogenous IL-6
520 ameliorated cold intolerance in cast-immobilized IL-6 KO mice via the
521 sympathetic nervous system. It may modulate thermal and energy homeostasis
522 through the fever response and metabolic regulation in multiple organs.
523 In conclusion, we have shown that cast immobilization induced
524 thermogenesis in BAT that was dependent on the utilization of free amino acids
525 derived from skeletal muscle, and that muscle-derived IL-6 stimulated BCAA
526 metabolism in skeletal muscle. Our findings may provide new insights into the
527 significance of skeletal muscle as a large reservoir of amino acids in the
528 regulation of body temperature. In addition, given that circulating levels of IL-6
529 or BCAAs are associated with obesity and diabetes,[46,47] IL-6–mediated BCAA
530 metabolism in skeletal muscle and BAT may also be associated with muscle
531 atrophy in metabolic diseases. Further investigation of IL-6–dependent amino
532 acid metabolism in BAT and skeletal muscle may inform the development of
533 preventive or therapeutic interventions for some forms of muscle atrophy.
534 Limitations of the study
535 Given that rodents are BAT-enriched mammals, whether BAT
536 thermogenesis is similarly activated in humans after skeletal muscle
537 immobilization remains to be investigated. Our study also did not determine the
538 mechanism underlying the induction of *Il6* expression in skeletal muscle by cast
539 immobilization. In addition, whereas muscle-derived IL-6 may stimulate protein
540 catabolism in immobilized muscle, the mechanism by which IL-6 increases
541 BCAA concentrations in skeletal muscle requires further investigation.
542
543

Methods

Mice

All experiments were approved by the Animal Care and Use Committee of Tokushima University and were conducted in accordance with the guidelines for the care and use of animals approved by the Council of the Physiological Society of Japana and ARRIVE guidelenies. Every effort was made to minimize animal suffering and to reduce the number of animals used in the experiments. All mice were housed at a constant room temperature of 23° ± 1°C and with a 12-h-light/12-h-dark cycle (lights on at 8.00 a.m.). They were fed standard nonpurified chow (Oriental Yeast) and had free access to both food and water. Our study examined male mice because male animals exhibited less variability in phenotype. Male mice at 9 to 13 weeks of age were studied. The mice were randomly assigned to experimental groups at the time of purchase or weaning. C57BL/6J mice were obtained from Japan SLC (Shizuoka, Japan), and IL-6 KO mice (B6;129S2-Il6<tm1kopf>) from RIKEN BRC through the National Bioresource Project of MEXT/AMED.[46] The IL-6 KO mice were maintained on the C57BL/6J background.

Cells

The mouse myoblast cell line C2C12 was obtained from American Type Culture Collection (CRL-1772™) and was maintained in Dulbecco's modified Eagle's medium (DMEM) containing 25 mM glucose (#D6429, Sigma) and supplemented with 10% fetal bovine serum (535-94155, BioSera) and 1% penicillin-streptomycin (15140-122, Gibco). After the cells had achieved 95% to 100% confluence, the culture medium was changed to DMEM containing 25 mM glucose and supplemented with 2% horse serum (16050-130, Thermo Fisher Scientific) and the cells were cultured for 5 days to promote their differentiation from myoblasts into myotubes. The myotubes were washed with phosphate-buffered saline (PBS) and then incubated in DMEM containing 25 mM glucose and supplemented with 1% bovine serum albumin (A8806-5G, Sigma) and 1% penicillin-streptomycin for 16 h before exposure to recombinant mouse IL-6 (rIL-6) at 50 ng/ml (575702, BioLegend) or vehicle (PBS) in the same medium for 1 h. The treated cells were washed with PBS or 5% mannitol solution and collected for RNA or metabolite extraction.

Mouse preadipocytes were obtained from Dr. Takeshi Yoneshiro the University of Tohoku, Tohoku, Japan[48] and were maintained in DMEM

580 containing 25 mM glucose and supplemented with 10% fetal bovine serum and
581 1% penicillin-streptomycin. After the cells had achieved 95% to 100%
582 confluence, they were induced to differentiate into brown adipocytes by
583 incubation in the same medium that was also supplemented with 1 nM
584 triiodothyronine (45006-44, Nacalai Tesque), insulin (093-06473, Wako) at 5
585 μg/ml, dexamethasone (11107-51, Nacalai Tesque) at 2 μg/ml, 0.5 mM
586 isobutylmethylxanthine (15879, Sigma), and 125 μM indomethacin (19233-51,
587 Nacalai Tesque). After culture for 2 days, the medium was replaced with DMEM
588 containing 25 mM glucose and supplemented with 10% fetal bovine serum, 1%
589 penicillin-streptomycin, and insulin (5 μg/ml), and the cells were maintained in
590 this medium with medium replenishment every 2 days. The cells were fully
591 differentiated at 6 to 7 days after the induction of differentiation. For
592 experiments, the brown adipocytes were washed with PBS at 7 days after
593 differentiation initiation and then incubated in DMEM containing 25 mM glucose
594 and supplemented with 1% bovine serum albumin and 1% penicillin-
595 streptomycin for 12 h before exposure to rIL-6 (50 ng/ml), 1 μM CL316 243
596 (Ab144605, Abcam), both agents, or vehicle (PBS). The treated cells were
597 collected after 24 h for RNA extraction.
598
599 **Cast immobilization**
600 Mice were subjected to bilateral or unilateral cast immobilization of hind limbs,
601 and unfixed mice were studied as controls. In brief, mice were lightly
602 anesthetized with inhalational isoflurane (MSD Animal Health), and the hind
603 limbs were fixed in a natural position, with care taken to avoid skin irritation and
604 congestion. After casting, the mice were housed individually with free access to
605 standard mouse chow and water. The mice out of cast immobilization were
606 excluded from experiments. In all experiments, mice were killed by cardiac
607 puncture after food deprivation for 3 h and tissue samples were collected.
608
609 **Surgical denervation of iBAT**
610 Surgical denervation of iBAT was performed on 9-week-old male mice as
611 described previously.[49] Animals were anesthetized by intraperitoneal injection of
612 domitor (Zenoaq) at a dose of 0.75 mg/kg, midazolam (Wako) at 4 mg/kg, and
613 butorphanol tartrate (Meiji Seika Pharma) at 5 mg/kg, and the incision site was
614 shaved and then disinfected with 0.05% chlorhexidine gluconate (5% Hibitane,
615 Sumitomo Pharma). A midline skin incision was made in the interscapular

616 region to expose both iBAT pads, the nerve fibers (five nerves per pad) were
617 identified and cut with sterile scissors, and the incision was closed with sutures.
618 For sham surgery, a skin incision was made and the medial side was gently
619 exposed. All mice were then individually housed in clean cages at room
620 temperature and were monitored daily. Cast immobilization was performed 1
621 week after surgery.
622
623 **Surgical removal of iBAT**
624 Surgical removal of iBAT was performed on 11-week-old male mice, with cast
625 immobilization being performed 1 week after surgery. Animals were
626 anesthetized and the incision site was shaved and disinfected as described for
627 iBAT denervation. A midline skin incision was made in the interscapular region,
628 all iBAT was removed, and the incision was closed with sutures. For sham
629 surgery, a skin incision was made and the medial side was gently exposed. All
630 mice were then housed individually in clean cages at room temperature.
631
632 **Acute cold tolerance test**
633 Core body temperature was measured with a Homeothermic Monitor (BWT-
634 100A, BRC) by gentle insertion of a thermal probe into the rectum of the mouse.
635 After recording of baseline body temperature at room temperature, animals
636 were placed in a cold chamber at 4°C for up to 4 h without access to food.
637 Tissue was then collected and snap-frozen.
638
639 **Treatment of mice with CL316 243 or rIL-6**
640 IL-6 KO mice with cast immobilization for 24 h were subjected to intraperitoneal
641 administration of 400 ng of rIL-6 (575702, BioLegend) in saline or of saline
642 alone. The mice were maintained sedentary for 3 h without access to food
643 before collection of tissue samples. Acute exposure to a cold environment
644 chamber was initiated 30 min after intraperitoneal treatment with rIL-6 (400 ng)
645 or saline in IL-6 KO mice or in C57BL/6J mice with denervated iBAT that had
646 been subjected to cast immobilization for 24 h. IL-6 KO mice with denervated
647 iBAT were treated intraperitoneally with CL316 243 (Ab144605, Abcam) at a
648 dose of 0.1 mg/kg, rIL-6 (400 ng), both agents, or saline vehicle, and tissue was
649 collected 3 h later. For long-term treatment of IL-6 KO mice with CL316 243, the
650 animals were injected intraperitoneally with the drug (0.1 mg/kg per day) or
651 saline for 7 days. Tissue was collected at 3 h after drug treatment on the last

652 day.
653
654 **Oxygen consumption and RER measurement**
655 Mice were acclimated to the analysis cage for 3 days before the start of
656 metabolic measurements. They were housed individually with free access to
657 food and water. Analysis of respiratory gases was performed with a mass
658 spectrometer (ARCO-2000, ARCO System). Measurements were performed for
659 seven consecutive days after cast immobilization.
660
661 **Locomotor activity recording**
662 The activity level of mice was assessed with an infrared activity monitor
663 (ACTIMO-100N, Shin Factory). A cage containing one mouse was placed inside
664 the activity monitor with infrared beams at 20-mm intervals. Mouse movements
665 were counted every 0.5 s for 24 h. Recording was performed for seven
666 consecutive days after cast immobilization.
667
668 **RNA isolation and RT and real-time PCR analysis**
669 Total RNA was extracted from mouse tissues and cells with the use of RNAiso
670 (#9109, Takara Bio) and subjected to RT with the use of a TaKaRa PrimeScript
671 II 1st Stand cDNA Synthesis Kit (Takara Bio). The resulting cDNA was subjected
672 to real-time PCR analysis with Fast SYBR Green Master Mix (3485612, Applied
673 Biosystems) in a Step One Plus Real-Time PCR System (Applied Biosystems).
674 The abundance of target mRNAs was normalized by that of *Gapdh* mRNA. The
675 PCR primers are listed in Table S3.
676
677 **Protein extraction and immunoblot analysis**
678 Total protein was extracted from mouse tissues by homogenization in a lysis
679 solution consisting of 1 M Tris-HCL (pH 7.4), 0.1 M EDTA, 1% Nonidet P-40, 5
680 mM sodium pyrophosphate, and phosphatase (25955-24, Nacalai Tesque) and
681 protease (07575-51, Nacalai Tesque) inhibitor cocktails. The homogenate was
682 centrifuged at 15,000 × *g* for 15 min at 4°C, and the resulting supernatant was
683 assayed for protein concentration with a Pierce BCA Protein Assay Kit (Thermo
684 Fisher Scientific) and then subjected to SDS-polyacrylamide gel electrophoresis
685 on a 10% acrylamide/4% bisacrylamide gel. The separated proteins were
686 transferred to polyvinylidene difluoride membrane, which was then exposed to
687 5% dried skim milk for 1 h at room temperature before incubation with primary

688 antibodies including those to PGC-1α (A12348, Abclonal), to UCP1 (sc-293418,
689 Santa Cruz Biotechnology), and to GAPDH (CAB932Hu01, Cloud-Clone) for 16
690 h at 4°C. Immune complexes were detected with horseradish peroxidase–
691 conjugated secondary antibodies (458, MBL; 7076P2, Cell Signaling
692 Technology), enhanced chemiluminescence reagents (170-5061, Bio-Rad
693 Labotatories, Inc.), and an Amersham Imager 600 instrument (GE Healthcare).
694 Band intensity was quantified with ImageJ software.
695
696 **Histology**
697 BAT was fixed in formalin, sectioned, and stained with hematoxylin-eosin.
698
699 **Metabolomics analysis**
700 Targeted profiling of amino acid metabolites was performed by capillary
701 electrophoresis–time-of-flight mass spectrometry (CE-TOF/MS) with an Agilent
702 7100 CE system coupled to an Agilent 6230 TOF mass spectrometer (Agilent
703 Technologies) according to previously described methods.[50]
704
705 **Measurement of noradrenaline**
706 Tissue samples were homogenized in methanol containing internal standards
707 ((±)-Norepinephrine-D6 hydrochloride solution, Sigma-Ardrich). The mixture
708 was centrifuged at 4 °C, and the aqueous fraction was isolated and centrifuged
709 through an cosmonice filter W (06543-04, nacalai tesque). Noradrenaline
710 content of the supernatants was measured by high-performance liquid
711 chromatography (SHIMAZU) with a reversed-phase column (Cadenza CD-C18
712 MF 100 × 2 mm 3 μm, Imtakt) and tandem mass spectrometry (MS/MS) (API
713 3200, AB SCIEX). Data are analyzed using AnalystLauncher (AB SCIEX).
714
715 **Measurement of [^{3}H]leucine uptake**
716 Mice were deprived of food for 3 h before intravenous injection of L-[4,5-
717 ^{3}H(*N*)]leucine (NET1166, PerkinElmer) at a dose of 1 μCi/g. They were then
718 maintained in a resting state for 40 min until blood and tissue collection, with
719 perfusion being performed before tissue isolation. Isolated tissue was cut into
720 small pieces, which were then placed in a round-bottom polypropylene tube
721 before the addition of 500 μl of distilled water, 150 μl of 30% hydrogen peroxide
722 (Wako), and 150 μl of 2 M KOH (1310-58-3, Hayashi Pure Chemical) in 2-
723 propanol (000-64783, Kishida Chemical) and incubation at 65°C for 2 h. The

724 tissue lysate was neutralized with 30% acetic acid, and 1 ml of liquid scintillation
725 solubilizer (Soluen-350, PerkinElmer) was added to the sample before
726 incubation at 50°C for 5 h and the further addition of 5 ml of liquid scintillation
727 cocktail (Hionic-Flour, PerkinElmer). Leucine uptake in each organ was
728 quantified by measurement of radioactivity with a scintillation counter (LSC-
729 7400, Hitachi).
730
731 **Hepatic glycogen assay**
732 The liver was homogenized in ice-cold citrate buffer (pH 4.2) containing NaF
733 (2.5 g/l), the homogenate was centrifuged at 14,000 × *g* for 5 min at 4°C, and
734 the resulting supernatant was assayed for glycogen with an EnzyChrom
735 Glycogen Assay Kit (BioAssay Systems).
736
737 **ELISAs**
738 Blood samples were collected from the heart of mice that had been
739 anesthetized by intraperitoneal injection of domitor (Zenoaq) at a dose of 0.75
740 mg/kg, midazolam (Wako) at 4 mg/kg, and butorphanol tartrate (Meiji Seika
741 Pharma) at 5 mg/kg after food deprivation for 3 h, and they were centrifuged at
742 7500 × *g* for 10 min at 4°C to isolate serum. Serum IL-6 and TNF-α
743 concentrations were determined with enzyme-linked immunosorbent assay
744 (ELISA) kits (Legend Max Mouse IL-6 ELISA Kit, BioLegend, and Mouse TNF
745 Alpha Uncoated ELISA, Invitrogen, respectively). Serum noradrenaline was
746 extracted with the use of a cis-diol–specific affinity gel, acylated, enzymatically
747 converted, and then measured with an ELISA kit (Noradrenaline Research
748 ELISA, ImmuSmol). Serum corticosterone was determined with a
749 Corticosterone ELISA Kit (Enzo Life Sciences).
750
751 **Statistical analysis**
752 Data are presented as means ± SEM unless indicated otherwise and were
753 analyzed with statistical software (JMP or Statcel–The Useful Add-in Forms on
754 Excel 4th ed.). Comparisons between two groups were performed with the
755 paired or unpaired t test, as appropriate. Those among more than two groups
756 were performed with Dunnett's test, by one-way analysis of variance (ANOVA)
757 followed by the Tukey-Kramer test, or by two-way ANOVA followed by Tukey's
758 post hoc test or the post hoc paired/unpaired t test with Bonferroni's correction.
759 A two-tailed p value was calculated for all experiments, and a value of <0.05

760 was considered statistically significant.

761

Acknowledgements

We thank members of the Radioisotope Center of Tokushima University Graduate School for technical support with the tracer experiments; members of the Special Mission Center for Metabolome Analysis, School of Medical Nutrition, Faculty of Medicine, Tokushima University, for technical support with the metabolomics analysis; Yoichiro Iwakura (University of Tokyo) for permission to study the IL-6 KO mice; Kohta Onishi (University of Tokushima) for technical support with the LC/MS/MS analysis; and the Support Center for Advanced Medical Sciences at Tokushima University Graduate School of Biomedical Sciences for general technical support. This study was supported by Funds for the Development of Human Resources in Science and Technology from the Ministry of Education, Culture, Sports, Science, and Technology of Japan (MEXT) through the Home for Innovative Researchers and Academic Knowledge Users consortium, and by KAKENHI grants (21J14844 to Y.I.-M. , 23K19926 to Y.I.-M., 23K19926 to Y.I.-M., 22H03535 to H.S., and 21K11724 to R.T.) from the Japan Society for the Promotion of Science.

Auther Contributions

Y.I.-M., T.S., S.F., and M.T. conducted the experiments; R.T. and H.S. designed the experiments; Y.I.-M., R.T., and H.S. wrote the manuscript; Y.O.-O., T.Y., K.N., and M.K. provided conceptual advice on data interpretation.

Decompeting interests

The authors declare no competing interests.

Additional information

Supplementary data is available for this paper at https://

Correspondence and requests for materials should be addressed to Hitoshi Sakaue.

References

1. Tansey, E.A., Johnson, C.D. (2015) Recent advances in thermoregulation. Adv Physiol Educ. 39 (3):139-48
https://doi.org/10.1152/advan.00126.2014

2. Piscitiello, E., Herwig, A., Haugg, E., Schröder, B., Breves G., *et al*. (2021) Acclimation of intestinal morphology and function in Djungarian hamsters (Phodopus sungorus) related to seasonal and acute energy balance. J Exp Biol. 16;224(Pt 4): jeb232876
https://doi.org/10.1242/jeb.232876

3. Cannon, B., Nedergaard, J. (2004) Brown adipose tissue: function and physiological significance. Physiol Rev. 84(1): 277-359
https://doi.org/10.1152/physrev.00015.2003

4. Nowack, J., Giroud, S., Arnold, W., Ruf, T. (2017) Muscle Non-shivering Thermogenesis and Its Role in the Evolution of Endothermy. Front Physiol. 8: 889
https://doi.org/10.3389/fphys.2017.00889

5. Rowland, L. A., Bal, N. C., Kozak,L. P., Periasamy, M. (2015) Uncoupling Protein 1 and Sarcolipin Are Required to Maintain Optimal Thermogenesis, and Loss of Both Systems Compromises Survival of Mice under Cold Stress. J Biol Chem. 8;290(19):12282-9
https://doi.org/10.1074/jbc.M115.637603

6. Golozoubova, V., Hohtola, E., Matthias, A., Jacobsson, A., Cannon, B., Nedergaard, J. (2001) Only UCP1 can mediate adaptive nonshivering thermogenesis in the cold. FASEB J. 15(11):2048-50
https://doi.org/10.1096/fj.00-0536fje

7. Janovska, P., Zouhar, P., Bardova, K., Otahal, J., Vrbacky, M., *et al*. (2013) Impairment of adrenergically-regulated thermogenesis in brown fat of obesity-resistant mice is compensated by non-shivering thermogenesis in skeletal muscle. Mol Metab. 69:101683
https://doi.org/10.1016/j.molmet.2023.101683

8. Blondin, D.P., Frisch, F., Phoenix, S., Guérin, B., Turcotte, É. E., *et al*. (2017) Inhibition of Intracellular Triglyceride Lipolysis Suppresses Cold-Induced Brown Adipose Tissue Metabolism and Increases Shivering in Humans. Cell Metab. 25(2): 438-447
https://doi.org/10.1016/j.cmet.2016.12.005

9. Bertile, F., Habold, C., Maho, Y. L., Giroud, S. (2021) Body Protein Sparing in Hibernators: A Source for Biomedical Innovation. Front Physiol. 18:12:634953
https://doi.org/10.3389/fphys.2021.634953

10. Holeček, M. (2018) Branched-chain amino acids in health and disease: metabolism, alterations in blood plasma, and as supplements. Nutr Metab (Lond). 15:33
https://doi.org/10.1186/s12986-018-0271-1

11. Heine, M., Fischer, A.W., Schlein, C., Jung, C., Straub, L.G., *et al*. (2018) Lipolysis Triggers a Systemic Insulin Response Essential for Efficient Energy Replenishment of Activated Brown Adipose Tissue in Mice
Cell Metab. 28(4): 644-655.e4
https://doi.org/10.1016/j.cmet.2018.06.020

12. Padmini, P., Khedoe, S.J., Hoeke, G., Kooijman, S., Dijk, W. *et al*. (2015) Brown adipose tissue takes up plasma triglycerides mostly after lipolysis. J Lipid Res. 56(1): 51-9
https://doi.org/10.1194/jlr.M052746

13. Olsen, J.S., Aslund, A., Bokhari, M.H., Hutchison, D.S., Bengtsson, T. (2019) Acute β-adrenoceptor mediated glucose clearance in brown adipose tissue; a distinct pathway independent of functional insulin signaling. Mol Metab. 30:240-249
https://doi.org/10.1016/j.molmet.2019.10.004

14. Millis, E.L., Pierce, K.A., Jedrychowski, M.P., Garrity, R., Winther, S. *et al*. (2018) Accumulation of succinate controls activation of adipose tissue thermogenesis. Nature. 560(7716): 102-106

https://doi.org/10.1038/s41586-018-0353-2

15. Yoneshiro, T., Wang, Q., Tajima, K., Matsushita, M., Maki, H., *et al*. (2019) BCAA catabolism in brown fat controls energy homeostasis through SLC25A44. Nature. 572(7771): 614-619
https://doi.org/10.1038/s41586-019-1503-x

16. Yoneshiro, T., Kataoka, N., Walejko, J.M., Ikeda, K., Brown, Z. *et al*. (2021) Metabolic flexibility via mitochondrial BCAA carrier SLC25A44 is required for optimal fever. Elife. 10: e66865
https://doi.org/10.7554/elife.66865

17. Reddy, A., Bozi, L.H.M., Yaghi, O.K., Millis, E.L., Xiao, H., *et al*. (2020) pH-Gated Succinate Secretion Regulates Muscle Remodeling in Response to Exercise. Cell. 183(1):62-75. e17
https://doi.org/10.1016/j.cell.2020.08.039

18. de Oliveira Dos Santos A.R. de Oliveira Zanuso B. Miola V.F.B. *et al*. (2021) Adipokines, Myokines, and Hepatokines: Crosstalk and Metabolic Repercussions. Int J Mol Sci. 22(5): 2639
https://doi.org/10.3390/ijms22052639

19. Tanaka, T., Narazaki, M., Kishimoto, T. (2014) IL-6 in inflammation, immunity, and disease. Cold Spring Harb Perspect Biol. 6(10): a016295
https://doi.org/10.3390/ijms22052639

20. Pedersen, B.K., Febbraio, M.A. (2008) Muscle as an Endocrine Organ: Focus on Muscle-Derived Interleukin-6. Physiol Rev. 88(4): 1379-406
https://doi.org/10.1152/physrev.90100.2007

21. Qing, H., Desrouleaux, R., Israni-Winger, K., Mineur, Y.S., Fogelman, N., *et al*. (2020) Origin and Function of Stress-Induced IL-6 in Murine Models. Cell. 182(2): 372-387.e14
https://doi.org/10.1016/j.cell.2020.05.054

22. Chen, Q., Wang, W. C., Bruce, R., Li, H., Schleider, D.M., Mulbury, M.J. *et*

901 *al*. (2004) Central role of IL-6 receptor signal-transducing chain gp130 in
902 activation of L-selectin adhesion by fever-range thermal stress. Immunity. 20(1):
903 59-70
904 https://doi.org/10.1016/s1074-7613(03)00358-3
905
906 23. Serrano, A. L., Baeza-Raja, B., Perdiguero, E., Muñoz-Cánoves, M.P.
907 (2008) Interleukin-6 Is an Essential Regulator of Satellite Cell-Mediated Skeletal
908 Muscle Hypertrophy. Cell Metab. 7(1): 33-44
909 https://doi.org/10.1016/j.cmet.2007.11.011
910
911 24. Ellingsgaard, H., Hauselmann, I., Schuler, B., Habib, A.M., Baggio, L.L., *et*
912 *al*. (2011) Interleukin-6 enhances insulin secretion by increasing glucagon-like
913 peptide-1 secretion from L cells and alpha cells. Nat Med. 17(11): 1481-9
914 https://doi.org/10.1038/nm.2513
915
916 25. Knudsen, J. G., Murholm, M., Carey, A.L., Beins, R.S., Basse, A.L.,et al.
917 (2014) Role of IL-6 in exercise training- and cold-induced UCP1 expression in
918 subcutaneous white adipose tissue. PLoS One. 9(1): e84910
919 https://doi.org/10.1371/journal.pone.0084910
920
921 26. Hall, G. V., Steensberg, A., Sacchetti, M., Fischer, C., Keller, C., *et al*.
922 (2003) Interleukin-6 stimulates lipolysis and fat oxidation in humans. J Clin
923 Endocrinol Metab. 88(7): 3005-10
924 https://doi.org/10.1210/jc.2002-021687
925
926 27. Nonogaki, K., Fuller, G.M., Fuentes, N.L., Moser, A.H., Staprans, I., *et al*.
927 (1995) Interleukin-6 stimulates hepatic triglyceride secretion in rats.
928 Endocrinology. 136(5): 2143-9
929 https://doi.org/10.1210/endo.136.5.7720663
930
931 28. Kawanishi, N., Funakoshi, T., Machida, S. (2018) Time-course study of
932 macrophage infiltration and inflammation in cast immobilization-induced
933 atrophied muscle of mice. Muscle Nerve. 57(6): 1006-1013
934 https://doi.org/10.1002/mus.26061
935
936 29. Bartness, T.J., Vaughan, C.H., Song, C.K. (2010) Sympathetic and sensory

innervation of brown adipose tissue. Int J Obes (Lond). 34 Suppl 1(0 1): S36-42 https://doi.org/10.1038/ijo.2010.182

30. Wang, Z., Wang, Q.A., Liu, Y., Jiang, L. (2021) Energy metabolism in brown adipose tissue. FEBS J. 288(12): 3647-3662 https://doi.org/10.1111/febs.16015

31. Gazzola, R.F., Sala, R., Bussolati, O., Visigalli, R., Dall'Asta, V., *et al*. (2001) The adaptive regulation of amino acid transport system A is associated to changes in ATA2 expression. FEBS Lett. 490(1-2): 11-4 https://doi.org/10.1016/s0014-5793(01)02126-3

32. Gjymishka, A., Palii, S.S., Shan, J., Kilberg, M.S. (2008) Despite increased ATF4 binding at the C/EBP-ATF composite site following activation of the unfolded protein response, system A transporter 2 (SNAT2) transcription activity is repressed in HepG2 cells. J Biol Chem. 283(41): 27736-27747 https://doi.org/10.1074/jbc.m803781200

33. HUANG, Y. and CHUANG, D.T. (1999) Down-regulation of rat mitochondrial branched-chain 2-oxoacid dehydrogenase kinase gene expression by glucocorticoids. Biochem. J. 339: 503–510

34. Kobayashi, R., Shimomura, Y., Murakami, T., Nakai, N., Otsuka, M., *et al*. (1999) Hepatic branched-chain α-keto acid dehydrogenase complex in female rats: activation by exercise and starvation. J Nutr Sci Vitaminol 45: 303-9 https://doi.org/10.3177/jnsv.45.303

35. Fukuhara, D., Kanai, Y., Chairoungdua, A., Babu, E., Bessho, F., *et al*. (2007) Protein characterization of Na+-independent system l amino acid transporter 3 in mice: a potential role in supply of branched-chain amino acids under nutrient starvation. Am. J. Pathol. 170 (3): 888-89 https://doi.org/10.2353/ajpath.2007.060428

36. Rowland, L.A., Bal, N.C., Periasamy, M. (2015) The role of skeletal-muscle-based thermogenic mechanisms in vertebrate endothermy. Biol Rev Camb Philos Soc. 90(4): 1279-97

https://doi.org/10.1111/brv.12157

37. Zurlo, F., Larson, K., Bogardus, C., Ravussin, E. (1990) Skeletal muscle metabolism is a major determinant of resting energy expenditure. J Clin Invest. 86(5): 1423-7
https://doi.org/10.1172/jci114857

38. Murashige, D., Jang, C., Neinast, M., Edwards, J.J., Cowan, A., *et al*. (2020) Comprehensive quantification of fuel use by the failing and nonfailing human heart. Science. 370(6514): 364-368
https://doi.org/10.1126/science.abc8861

39. Bonetto, A., Aydogdu, T., Jin, X., Zhang, Z., Zhan, R.,*et al*. (2012) JAK/STAT3 pathway inhibition blocks skeletal muscle wasting downstream of IL-6 and in experimental cancer cachexia. Am J Physiol Endocrinol Metab 303: E410–E421
https://doi.org/10.1152/ajpendo.00039.2012

40. Zanders, L., Kny, M., Hahn, A., Schmidt, S., Wundersitz, S., *et al*. (2022) Sepsis induces interleukin 6, gp130/JAK2/STAT3, and muscle wasting. J Cachexia Sarcopenia Muscle. 2022; 13(1): 713-727
https://doi.org/10.1002/jcsm.12867

41. Hirata, Y., Nomura, K., Kato, D., Tachibana, Y., Niikura, T., *et al*. (2022) A Piezo1/KLF15/IL-6 axis mediates immobilization-induced muscle atrophy. J Clin Invest. 132(10): 1-13
https://doi.org/10.1172/jci154611

42. Bustamante, M., Fernández-Verdejo, R., Jaimovich, E., Buvinic, S. (2014) Electrical stimulation induces IL-6 in skeletal muscle through extracellular ATP by activating Ca (2+) signals and an IL-6 autocrine loop. Am J Physiol Endocrinol Metab. 306(8): E869-82
https://doi.org/10.1152/ajpendo.00450.2013

43. Tomiya, S., Tamura, Y., Kouzaki, K., Kotani, T., Wakabayashi, Y., *et al*. (2019) Cast immobilization of hindlimb upregulates sarcolipin expression in

atrophied skeletal muscles and increases thermogenesis in C57BL/6J mice. Am J Physiol Regul Integr Comp Physiol. 317(5): R649-R661
https://doi.org/10.1152/ajpregu.00118.2019

44. Poller, W.C., Downey, J., Mooslechner, A.A., Khan, N., Li, L., *et al*. (2022) Brain motor and fear circuits regulate leukocytes during acute stress. Nature. 607(7919): 578-584
https://doi.org/10.1038/s41586-022-04890-z

45. Cheng, Y., Jope, R.S., Beurel, E. (2015) A pre-conditioning stress accelerates increases in mouse plasma inflammatory cytokines induced by stress. BMC Neurosci. 16:31
https://doi.org/10.1186/s12868-015-0169-z

46. Wallenius, V., Wallenius, K., Ahrén, B., Rudling, M., Carlsten, H., *et al*. (2002) Interleukin-6-deficient mice develop mature-onset obesity. Nat Med. 8(1): 75-9
https://doi.org/10.1038/nm0102-75

47. Wang, T.J., Larson, M.G., Vasan, R.S., Cheng, S., Rhee, E.P. *et al*. (2011) Metabolite profiles and the risk of developing diabetes. Nat Med. 17(4): 448-53
https://doi.org/10.1038/nm.2307

48. Shinoda, K., Luijten, I.H.N., Hasegawa, Y., Hong, H., Sonne, S.B., *et al*. (2015) Genetic and functional characterization of clonally derived adult human brown adipocytes. Nat Med. 21(4):389-94
https://doi.org/10.1038/nm.3819

49. Vaughan, C.H., Zarebidaki, E., Ehlen, J.C., Bartness, T.J. (2014) Analysis and measurement of the sympathetic and sensory innervation of white and brown adipose tissue. Methods Enzymol. 537: 199-225
https://doi.org/10.1016/b978-0-12-411619-1.00011-2

50. Okamatsu-Ogura, Y., Kuroda, M., Tsutsumi, R., Tsubota, A., Saito, M., *et al*. (2020) UCP1-dependent and UCP1-independent metabolic changes induced by acute cold exposure in brown adipose tissue of mice. Metabolism. 113: 154396

https://doi.org/10.1016/j.metabol.2020.154396

1049 **Figure Legends**

1050 **Figure 1. Cast immobilization suppresses muscle thermogenesis and**
1051 **induces BAT thermogenesis via sympathetic activation**

1052 (A) Time course of rectal core body temperature of cast-immobilized (gypsum, n
1053 = 6) and control (n = 5) mice subjected to a cold (4°C) challenge test. The test
1054 was performed 7 days after bilateral immobilization of hind limbs.
1055 (B) Rectal core body temperature of cast-immobilized (n = 5) and control (n = 5)
1056 mice during cold (4°C) exposure at 24 h after bilateral cast immobilization.
1057 (C) Decline in rectal temperature of cast-immobilized and control (n = 9) mice
1058 after cold (4°C) exposure for 4 h performed 2 h after unilateral (UL, n =8) or
1059 bilateral (BL, n = 9) immobilization.
1060 (D) Rectal core body temperature of cast-immobilized (n = 6) and control (n = 4)
1061 mice at room temperature after bilateral cast immobilization.
1062 (E–G) Immunoblot analysis of PGC-1α (n = 3 or 4 per group) and UCP1 (n = 6
1063 per group) in iBAT of control mice and mice subjected to bilateral cast
1064 immobilization for the indicated times. GAPDH was examined as a loading
1065 control. Representative blots (E) and densitometric quantitation of the PGC-
1066 1α/GAPDH (F) and UCP1/GAPDH (G) band intensity ratios are shown.
1067 (H) Reverse transcription (RT) and real-time polymerase chain reaction (PCR)
1068 analysis of the *Ucp1/Gapdh* mRNA abundance ratio in iBAT of control mice and
1069 mice subjected to bilateral cast immobilization for the indicated times (n = 7 to
1070 13 per group).
1071 (I) Noradrenaline concentrations in iBAT of cast-immobilized (n = 4) and control
1072 (n = 4) mice at 24 h after subsequent biteral cast immobilization.
1073 (J) RT and real-time PCR analysis of the *Ucp1/Gapdh* mRNA abundance ratio
1074 in iBAT subjected to surgical denervation or sham surgery, either in control mice
1075 or in mice at 24 h after subsequent bilateral cast immobilization (n = 6–9 per
1076 group).
1077 (K) Rectal core body temperature of mice as in (I) subjected to cold (4°C)
1078 exposure for 1 h (n = 3 or 4 per group).
1079 All quantitative data are means ± SEM. *$p < 0.05$, **$p < 0.01$ as determined by
1080 two-way ANOVA followed by Tukey's post hoc test or the post hoc
1081 paired/unpaired t test with Bonferroni's correction (A, B, D, and K), by one-way
1082 ANOVA followed by Tukey's post hoc test (C and J), by Dunnett's test (F-H), or
1083 by the unpaired t test (I)
1084 See also Figure 1_figure supplement 1 and 2, and Table S1.

1085

1086 **Figure 2. Cast immobilization alters systemic metabolic dynamics**
1087 **associated with BAT thermogenesis**
1088 (A and B) Concentrations of carbohydrate metabolites (A) and amino acids (B)
1089 in sham-operated or denervated iBAT of mice without (control) or at the
1090 indicated times after bilateral cast immobilization. The metabolomics data are
1091 presented as heat maps corresponding to the $\log_{10}$ value of fold change in cast-
1092 immobilized mice relative to the corresponding control mice and are means of
1093 four or five mice in each group. TCA, tricarboxylic acid cycle.
1094 (C and D) RT and real-time PCR analysis of mRNA abundance for the fatty acid
1095 transporter CD36 and the succinate transporter SLC25A10 in sham-operated or
1096 denervated iBAT of control mice or mice subjected to bilateral cast
1097 immobilization for 24 h (n = 6 per group).
1098 (E) Succinate content of sham-operated or denervated iBAT of control mice or
1099 mice subjected to bilateral cast immobilization for 24 h (n = 3–5 per group).
1100 (F and G) Oxygen consumption rate (VO_2) and respiratory exchange ratio
1101 (RER), respectively, for control mice and mice subjected to bilateral cast
1102 immobilization for 7 days (n = 6 per group).
1103 (H) Weight of eWAT for control mice and mice subjected to bilateral cast
1104 immobilization for the indicated times (n = 5–7 per group).
1105 (I) Hepatic glycogen content for control mice and mice subjected to bilateral
1106 cast immobilization for the indicated times (n = 6–10 per group).
1107 Date in (C) through (I) are means ± SEM. *$p < 0.05$, **$p < 0.01$ as determined
1108 by one-way ANOVA followed by Tukey's post hoc test (C–E), by two-way
1109 ANOVA followed by Tukey's post hoc test or the unpaired post hoc t test with
1110 Bonferroni's correction (F and G), or by Dunnett's test (H and I).
1111 See also Figure 2_figure supplement 1.
1112

1113 **Figure 3. Free amino acids are transferred from skeletal muscle to BAT**
1114 **and the liver for maintenance of energy homeostasis**
1115 (A and B) Metabolomics analysis of amino acid concentrations in soleus and
1116 EDL muscles (A) as well as in serum and the liver (B) of control mice and mice
1117 subjected to bilateral cast immobilization for the indicated times. Results are
1118 presented as heat maps of the $\log_{10}$ value of fold change for cast-immobilized
1119 mice relative to control mice and are means of three mice per group.
1120 (C) RT and real-time PCR analysis of gene expression for SLC transporters and

1121 mitochondrial BCAA catabolic enzymes in iBAT, liver, and soleus of control mice
1122 and mice subjected to bilateral cast immobilization for the indicated times.
1123 Results are presented as heat maps of the $\log_{10}$ value of fold change for cast-
1124 immobilized mice relative to control mice and are are shown individually for
1125 three to six mice of each group.
1126 (D) Organ-specific [^{3}H]leucine uptake in control mice and mice subjected to
1127 bilateral cast immobilization for 24 h (n = 4–6 per group). sWAT, subcutaneous
1128 WAT.
1129 (E) RT and real-time PCR analysis of SLC25A44 gene expression in sham-
1130 operated or denervated iBAT of control mice and mice subjected to subsequent
1131 bilateral cast immobilization for 24 h (n = 6 per group).
1132 Data in (D) and (E) are means ± SEM. *p < 0.05, **p < 0.01 as determined by
1133 the unpaired t test (D) or by one-way ANOVA followed by Tukey's post hoc test
1134 (E).
1135 See also Figure 3_figure supplement 1.
1136
1137 **Figure 4. Cast immobilization upregulates *Il6* expression in BAT and**
1138 **skeletal muscle**
1139 (A and B) RT and real-time PCR analysis of IL-1β, IL-6, IL-10, IL-15, TNF-α,
1140 MCP-1, BMP8B, FGF21, and irisin gene expression in iBAT (A) or soleus (B) of
1141 control mice or mice at 10 h (iBAT) or 24 h (soleus) after bilateral cast
1142 immobilization (n = 5 or 6 per group).
1143 (C and D) RT and real-time PCR analysis of *Il6* expression in iBAT (C) and
1144 soleus (D) of control mice and mice at the indicated times after bilateral cast
1145 immobilization (n = 3–7 per group).
1146 (E–L) RT and real-time PCR analysis of *Saa3* (E, G, I, and K) and *Socs3* (F, H,
1147 J, and L) mRNA abundance in iBAT (E and F), soleus (G and H), liver (I and J),
1148 and eWAT (K and L) of control mice and mice at the indicated times after
1149 bilateral cast immobilization (n = 3–7 per group)
1150 (M) RT and real-time PCR analysis of *Il6* expression, respectively, in denervated
1151 iBAT of control mice or mice at the indicated times after bilateral cast
1152 immobilization (n = 4-7 per group).
1153 (N) Serum IL-6 concentration in control mice or mice at the indicated times after
1154 bilateral cast immobilization (n = 6 per group).
1155 All data are means ± SEM. *p < 0.05, **p < 0.01, NS (not significant) as
1156 determined by the unpaired t test (A and B) or by Dunnett's test (C–N).

1157 See also Figure 4_figure supplement 1.
1158
1159 **Figure 5. IL-6 affects energy metabolism in BAT and skeletal muscle of**
1160 **cast-immobilized mice**
1161 (A) Change in rectal body temperature during cold exposure at 4°C for 4 h for
1162 WT (n = 4 or 5) and IL-6 KO (n = 4 or 5) mice that had been subjected (or not)
1163 to bilateral cast immobilization for 24 h.
1164 (B and C) Concentrations of carbohydrate metabolites (B) and amino acids (C)
1165 in iBAT of IL-6 KO (–/–) and WT (+/+) mice without (control) or with bilateral cast
1166 immobilization for the indicated times. Results are presented as heat maps of
1167 the $\log_{10}$ value of the fold change relative to control WT mice and are means of
1168 four mice in each group.
1169 (D–F) RT and real-time PCR analysis of the expression of SLC25A44 (D),
1170 BCKDHA (E), and CD36 (F) genes in iBAT of IL-6 KO and WT mice without
1171 (control) or with bilateral cast immobilization for 24 h (n = 5 or 6).
1172 (G) Incorporation of [^{3}H]leucine in iBAT of IL-6 KO and WT mice without
1173 (control) or with bilateral cast immobilization for 24 h (n = 4 or 5 per group).
1174 (H–J) BCAA (Val, Ile, and Leu, respectively) concentrations in soleus of IL-6 KO
1175 and WT mice without (control) or with bilateral cast immobilization for 1 or 7
1176 days (n = 4 per group).
1177 Data in (A) and (D) through (J) are means ± SEM. *$p < 0.05$, **$p < 0.01$ as
1178 determined by one-way ANOVA followed by Tukey's post hoc test (D–G), by
1179 Dunnett's test (H–J), or by two-way ANOVA followed by Tukey's post hoc test
1180 (A).
1181 See also Figure 5_figure supplement 1.
1182
1183 **Figure 6. Skeletal-muscle-derived IL-6 increases BCAA concentrations in**
1184 **skeletal muscle for support of BAT thermogenesis**
1185 (A–C) Concentrations of BCAAs (Val, Ile, and Leu, respectively) in the soleus of
1186 control IL-6 KO mice and at 3 h after intraperitoneal administration of
1187 recombinant IL-6 (rIL-6, 400 ng) or vehicle in IL-6 KO mice that had been
1188 subjected to bilateral cast immobilization for 24 h (n = 4 or 5 per group).
1189 (D) BCAA concentrations in C2C12 myotubes incubated in the absence or
1190 presence of rIL-6 (50 ng/ml) for 1 h (n = 6 independent experiments) .
1191 (E) Rectal core body temperature during cold exposure at 4°C for 1 h for control
1192 IL-6 KO mice and for IL-6 KO mice subjected to bilateral cast immobilization for

1193 24 h and injected intraperitoneally with rIL-6 (400 ng) or vehicle 30 min before
1194 cold challenge (n = 5 per group).
1195 (F) Rectal core body temperature during cold exposure at 4°C for 1 h for
1196 C57BL/6J mice with denervated iBAT subjected or not to bilateral cast
1197 immobilization and treatment with rIL-6 or vehicle as in (E) (n = 4 per group).
1198 (G) Serum IL-6 concentration of mice subjected to surgical removal of iBAT and
1199 then subjected (or not, control) to bilateral cast immobilization for the indicated
1200 times (n = 4-6 per group).
1201 (H) Weight of eWAT in mice subjected to surgical removal of iBAT (or to sham
1202 surgery) followed (or not, control) by bilateral cast immobilization for 7 days (n =
1203 5-7 per group).
1204 (I-K) Concentrations of BCAAs (Val, Ile, and Leu, respectively) in soleus of mice
1205 subjected to surgical removal of iBAT and then subjected (or not, control) to
1206 bilateral cast immobilization for the indicated times (n = 4 per group).
1207 (L) RT and real-time PCR analysis of *Il6* expression in iBAT, soleus, liver, eWAT,
1208 and spleen of mice subjected (or not) to cold (4°C) exposure for 4 h (control, n =
1209 6–9; cold exposure, n = 5 or 6).
1210 (M and N) RT and real-time PCR analysis of *Saa3* (M) and *Socs3* (N) mRNA
1211 abundance in soleus of mice subjected (or not) as (L) (control, n = 6; cold
1212 exposure, n = 5).
1213 (O) Amino acid concentrations in soleus of WT (+/+) and IL-6 KO (–/–) mice
1214 subjected (or not) to cold exposure at 4°C for 4 h. Results are presented as
1215 heat maps of the $\log_{10}$ value of fold change relative to WT control mice and are
1216 means of four mice in each group.
1217 (P) Valine concentration in soleus of WT and IL-6 KO mice subjected (or not) to
1218 cold exposure at 4°C for 4 h (n = 4 per group).
1219 All data other than those in (O) are means ± SEM. *p < 0.05, **p < 0.01, NS (not
1220 significant) as determined by Dunnett's test (A–C and G and I-K), or by the
1221 unpaired t test (D and L-N) or by one-way ANOVA followed by Tukey's post hoc
1222 test (H and P), or by two-way ANOVA followed by the post hoc paired/unpaired t
1223 test with Bonferroni's correction (E and F),
1224 See also Figure 6_figure supplement 1 and 2.
1225

Fig.1

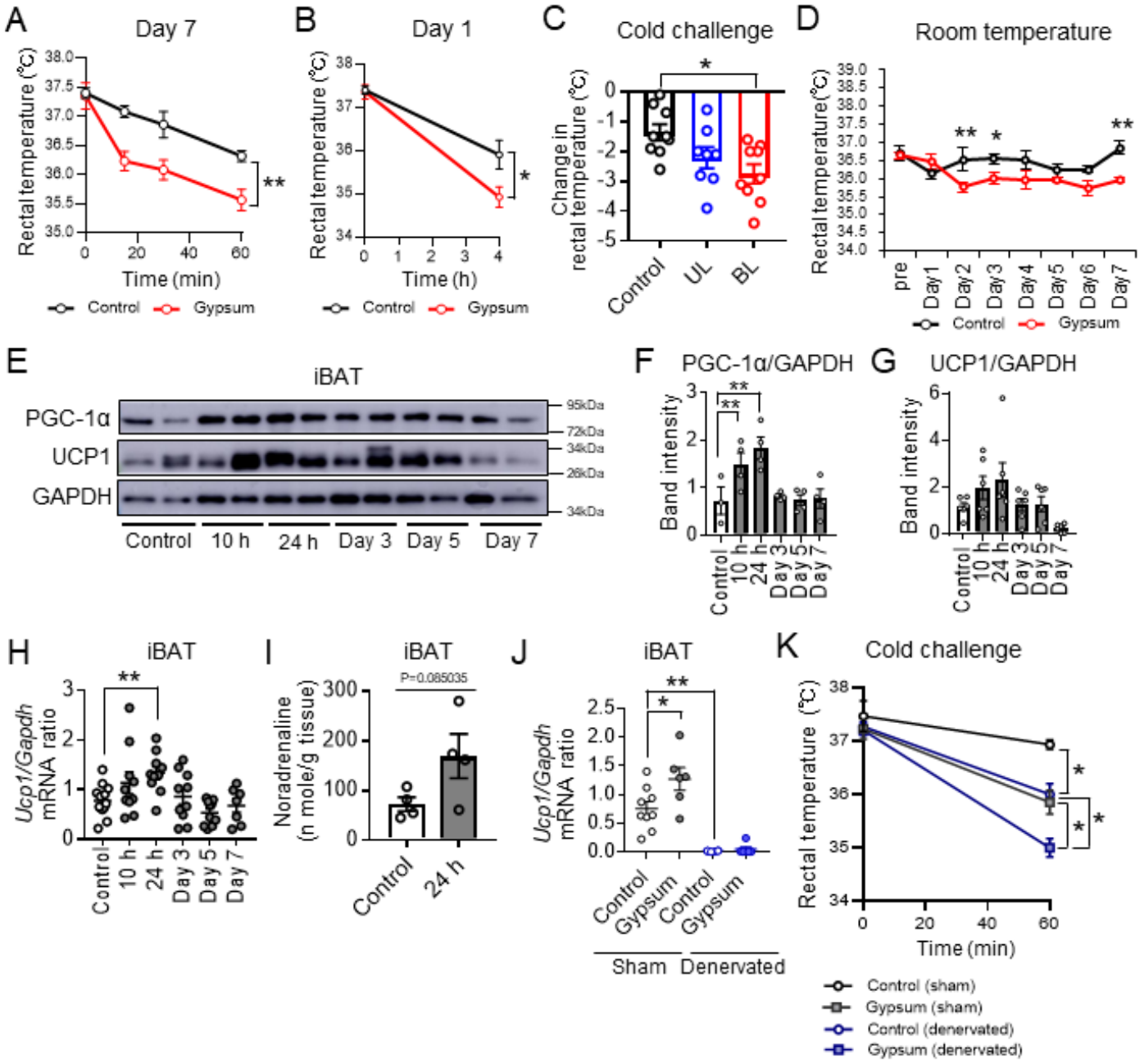
A
Day 7
Rectal temperature (℃)
Time (min)
Control
Gypsum
B
Day 1
Rectal temperature (℃)
Time (h)
C
Cold challenge
Change in rectal temperature (℃)
Control
UL
BL
D
Room temperature
Rectal temperature(℃)
pre
Day1
Day2
Day3
Day4
Day5
Day6
Day7
E
iBAT
PGC-1α
UCP1
GAPDH
95kDa
72kDa
34kDa
26kDa
34kDa
Control
10 h
24 h
Day 3
Day 5
Day 7
F
PGC-1α/GAPDH
Band intensity
G
UCP1/GAPDH
H
iBAT
Ucp1/Gapdh mRNA ratio
I
iBAT
P=0.085035
Noradrenaline (n mole/g tissue)
J
iBAT
Ucp1/Gapdh mRNA ratio
Sham
Denervated
K
Cold challenge
Rectal temperature (℃)
Time (min)
Control (sham)
Gypsum (sham)
Control (denervated)
Gypsum (denervated)

Fig.2

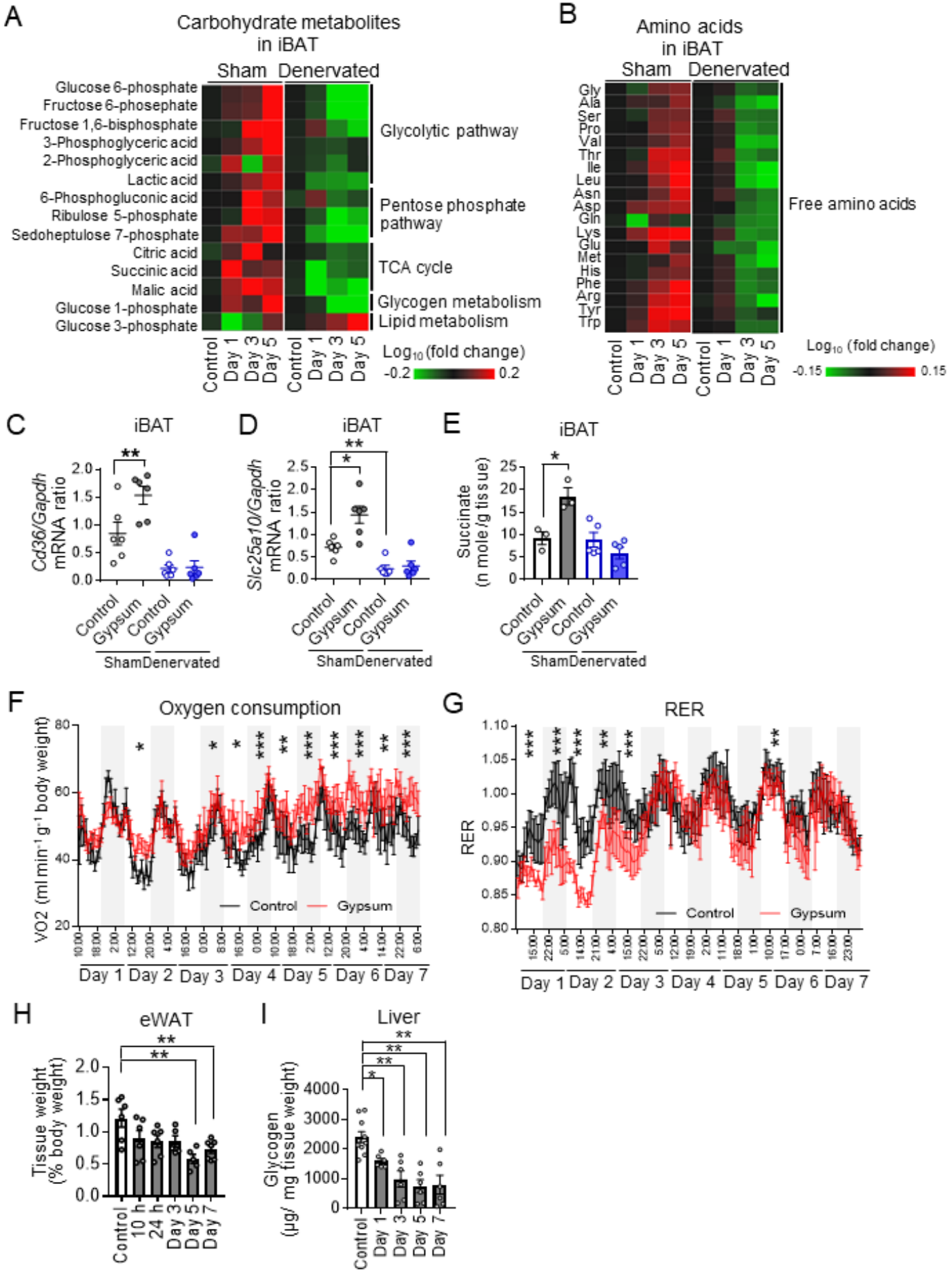
A
Carbohydrate metabolites in iBAT
Sham Denervated
Glucose 6-phosphate
Fructose 6-phosephate
Fructose 1,6-bisphosphate
3-Phosphoglyceric acid
2-Phosphoglyceric acid
Lactic acid
6-Phosphogluconic acid
Ribulose 5-phosphate
Sedoheptulose 7-phosphate
Citric acid
Succinic acid
Malic acid
Glucose 1-phosphate
Glucose 3-phosphate
Glycolytic pathway
Pentose phosphate pathway
TCA cycle
Glycogen metabolism
Lipid metabolism
Control Day 1 Day 3 Day 5 Control Day 1 Day 3 Day 5
Log10 (fold change)
-0.2 0.2
B
Amino acids in iBAT
Sham Denervated
Gly Ala Ser Pro Val Thr Ile Leu Asn Asp Gln Lys Glu Met His Phe Arg Tyr Trp
Free amino acids
Control Day 1 Day 3 Day 5 Control Day 1 Day 3 Day 5
Log10 (fold change)
-0.15 0.15
C
iBAT
Cd36/Gapdh mRNA ratio
Control Gypsum Control Gypsum
Sham Denervated
D
iBAT
Slc25a10/Gapdh mRNA ratio
Control Gypsum Control Gypsum
Sham Denervated
E
iBAT
Succinate (n mole/g tissue)
Control Gypsum Control Gypsum
Sham Denervated
F
Oxygen consumption
VO2 (ml min-1 g-1 body weight)
Control Gypsum
Day 1 Day 2 Day 3 Day 4 Day 5 Day 6 Day 7
G
RER
Control Gypsum
Day 1 Day 2 Day 3 Day 4 Day 5 Day 6 Day 7
H
eWAT
Tissue weight (% body weight)
Control 10 h 24 h Day 3 Day 5 Day 7
I
Liver
Glycogen (μg/ mg tissue weight)
Control Day 1 Day 3 Day 5 Day 7

Fig.3

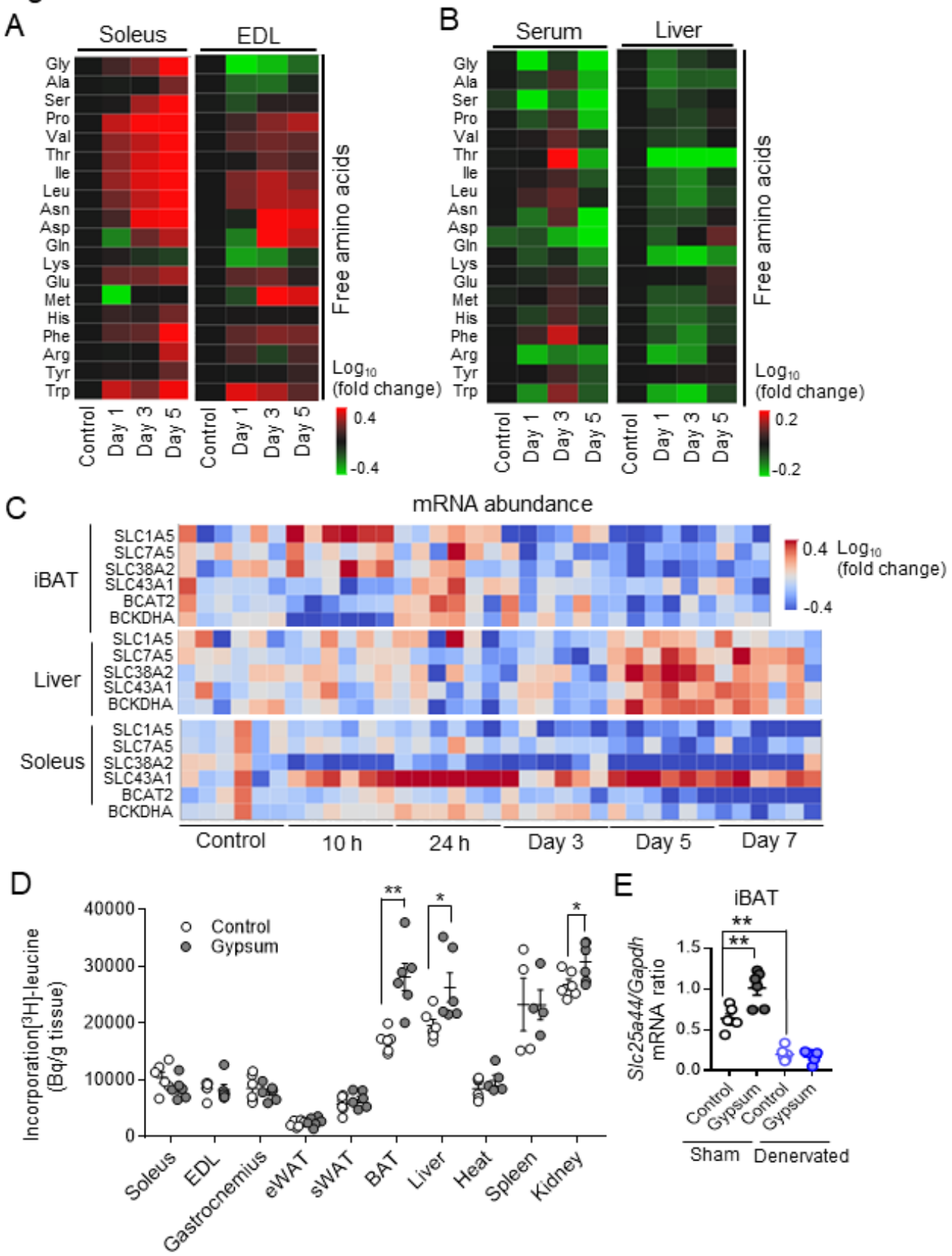
A
Soleus
EDL
Gly
Ala
Ser
Pro
Val
Thr
Ile
Leu
Asn
Asp
Gln
Lys
Glu
Met
His
Phe
Arg
Tyr
Trp
Free amino acids
Log10 (fold change)
0.4
-0.4
Control
Day 1
Day 3
Day 5
B
Serum
Liver
0.2
-0.2
C
mRNA abundance
iBAT
Liver
Soleus
SLC1A5
SLC7A5
SLC38A2
SLC43A1
BCAT2
BCKDHA
Control
10 h
24 h
Day 3
Day 5
Day 7
D
Incorporation[3H]-leucine (Bq/g tissue)
Control
Gypsum
40000
30000
20000
10000
0
Soleus
EDL
Gastrocnemius
eWAT
sWAT
BAT
Liver
Heat
Spleen
Kidney
E
iBAT
Slc25a44/Gapdh mRNA ratio
1.5
1.0
0.5
0.0
Sham
Denervated

Fig.4

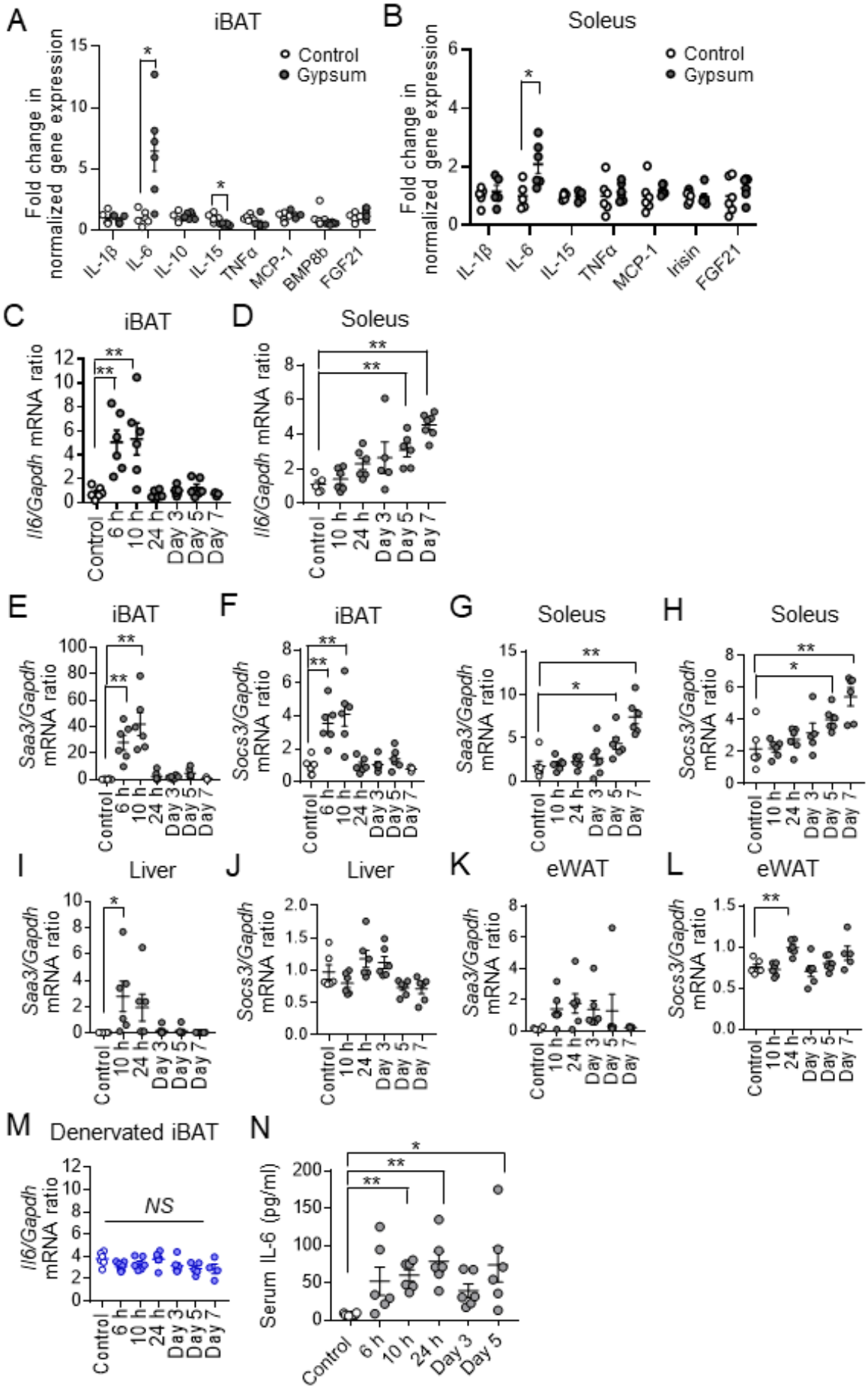
A
iBAT
Control
Gypsum
Fold change in normalized gene expression
IL-1β
IL-6
IL-10
IL-15
TNFα
MCP-1
BMP8b
FGF21
B
Soleus
Irisin
C
iBAT
Il6/Gapdh mRNA ratio
Control
6 h
10 h
24 h
Day 3
Day 5
Day 7
D
Soleus
E
iBAT
Saa3/Gapdh mRNA ratio
F
iBAT
Socs3/Gapdh mRNA ratio
G
Soleus
H
Soleus
I
Liver
J
Liver
K
eWAT
L
eWAT
M
Denervated iBAT
NS
N
Serum IL-6 (pg/ml)

Fig.5

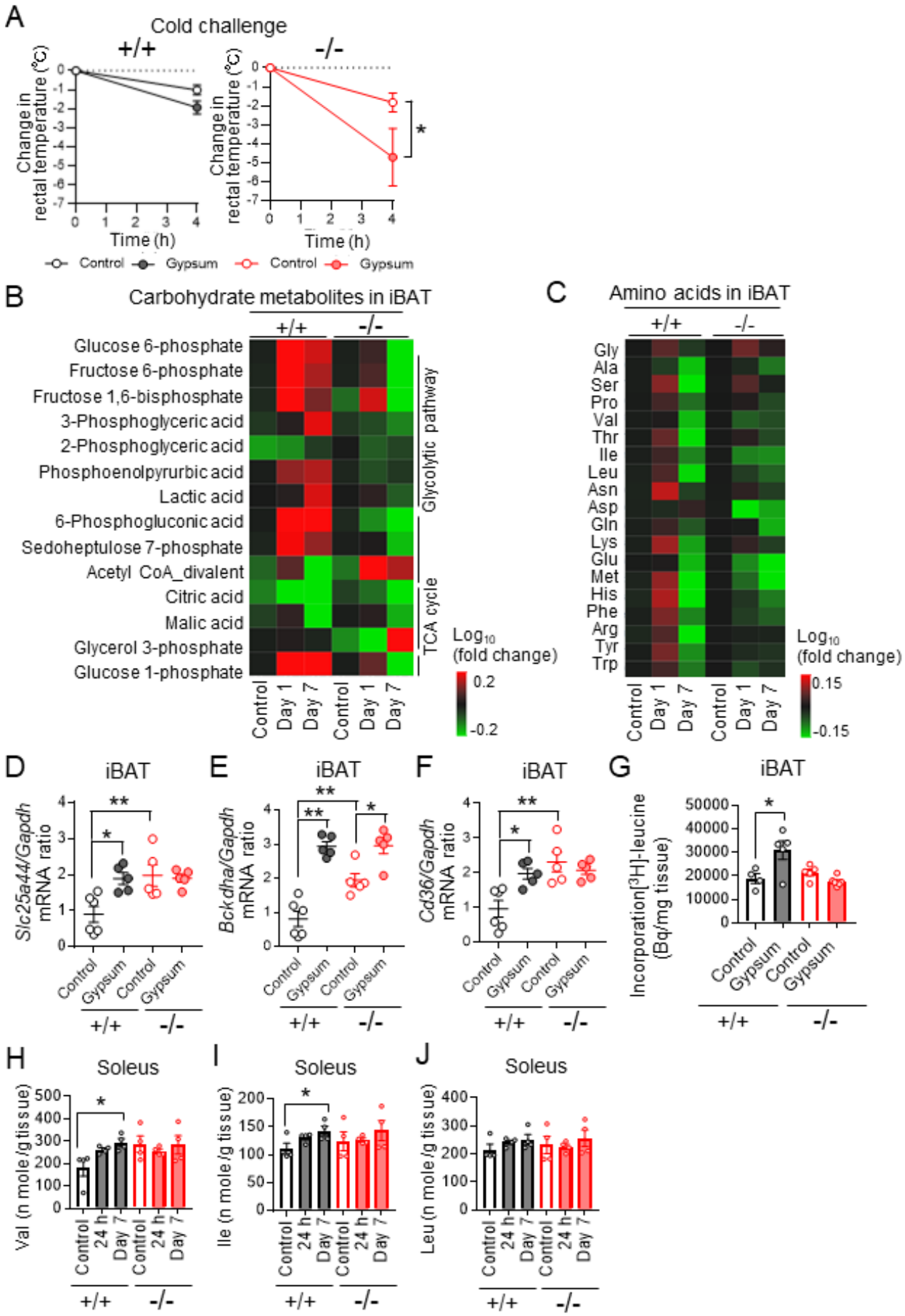
A
Cold challenge
+/+
-/-
Change in rectal temperature (°C)
Time (h)
Control
Gypsum
B
Carbohydrate metabolites in iBAT
Glucose 6-phosphate
Fructose 6-phosphate
Fructose 1,6-bisphosphate
3-Phosphoglyceric acid
2-Phosphoglyceric acid
Phosphoenolpyrurbic acid
Lactic acid
6-Phosphogluconic acid
Sedoheptulose 7-phosphate
Acetyl CoA_divalent
Citric acid
Malic acid
Glycerol 3-phosphate
Glucose 1-phosphate
Glycolytic pathway
TCA cycle
Control
Day 1
Day 7
Log10 (fold change)
C
Amino acids in iBAT
Gly
Ala
Ser
Pro
Val
Thr
Ile
Leu
Asn
Asp
Gln
Lys
Glu
Met
His
Phe
Arg
Tyr
Trp
D
iBAT
Slc25a44/Gapdh mRNA ratio
E
Bckdha/Gapdh mRNA ratio
F
Cd36/Gapdh mRNA ratio
G
Incorporation[3H]-leucine (Bq/mg tissue)
H
Soleus
Val (n mole/g tissue)
I
Ile (n mole/g tissue)
J
Leu (n mole/g tissue)
24 h

Fig.6

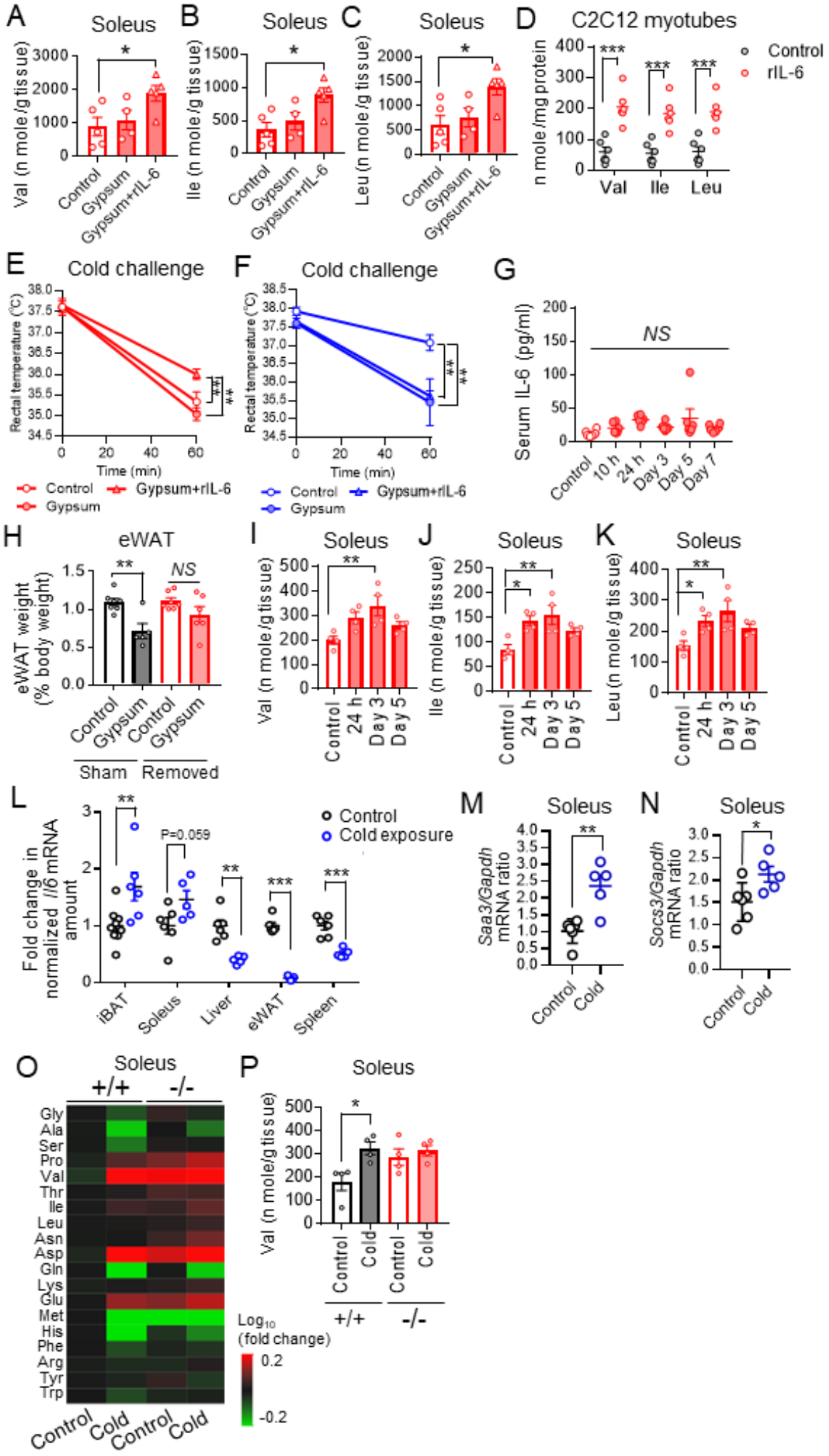
A
Soleus
Val (n mole/g tissue)
Control
Gypsum
Gypsum+rIL-6
B
Soleus
Ile (n mole/g tissue)
C
Soleus
Leu (n mole/g tissue)
D
C2C12 myotubes
n mole/mg protein
Control
rIL-6
Val
Ile
Leu
E
Cold challenge
Rectal temperature (°C)
Time (min)
Control
Gypsum
Gypsum+rIL-6
F
Cold challenge
Rectal temperature (°C)
Time (min)
Control
Gypsum
Gypsum+rIL-6
G
Serum IL-6 (pg/ml)
NS
Control
10 h
24 h
Day 3
Day 5
Day 7
H
eWAT
eWAT weight (% body weight)
NS
Control
Gypsum
Control
Gypsum
Sham
Removed
I
Soleus
Val (n mole/g tissue)
Control
24 h
Day 3
Day 5
J
Soleus
Ile (n mole/g tissue)
Control
24 h
Day 3
Day 5
K
Soleus
Leu (n mole/g tissue)
Control
24 h
Day 3
Day 5
L
Fold change in normalized Il6 mRNA amount
P=0.059
Control
Cold exposure
iBAT
Soleus
Liver
eWAT
Spleen
M
Soleus
Saa3/Gapdh mRNA ratio
Control
Cold
N
Soleus
Socs3/Gapdh mRNA ratio
Control
Cold
O
Soleus
+/+
-/-
Gly
Ala
Ser
Pro
Val
Thr
Ile
Leu
Asn
Asp
Gln
Lys
Glu
Met
His
Phe
Arg
Tyr
Trp
Control
Cold
Control
Cold
Log10 (fold change)
0.2
-0.2
P
Soleus
Val (n mole/g tissue)
Control
Cold
Control
Cold
+/+
-/-

Fudure1_figure supplement 1

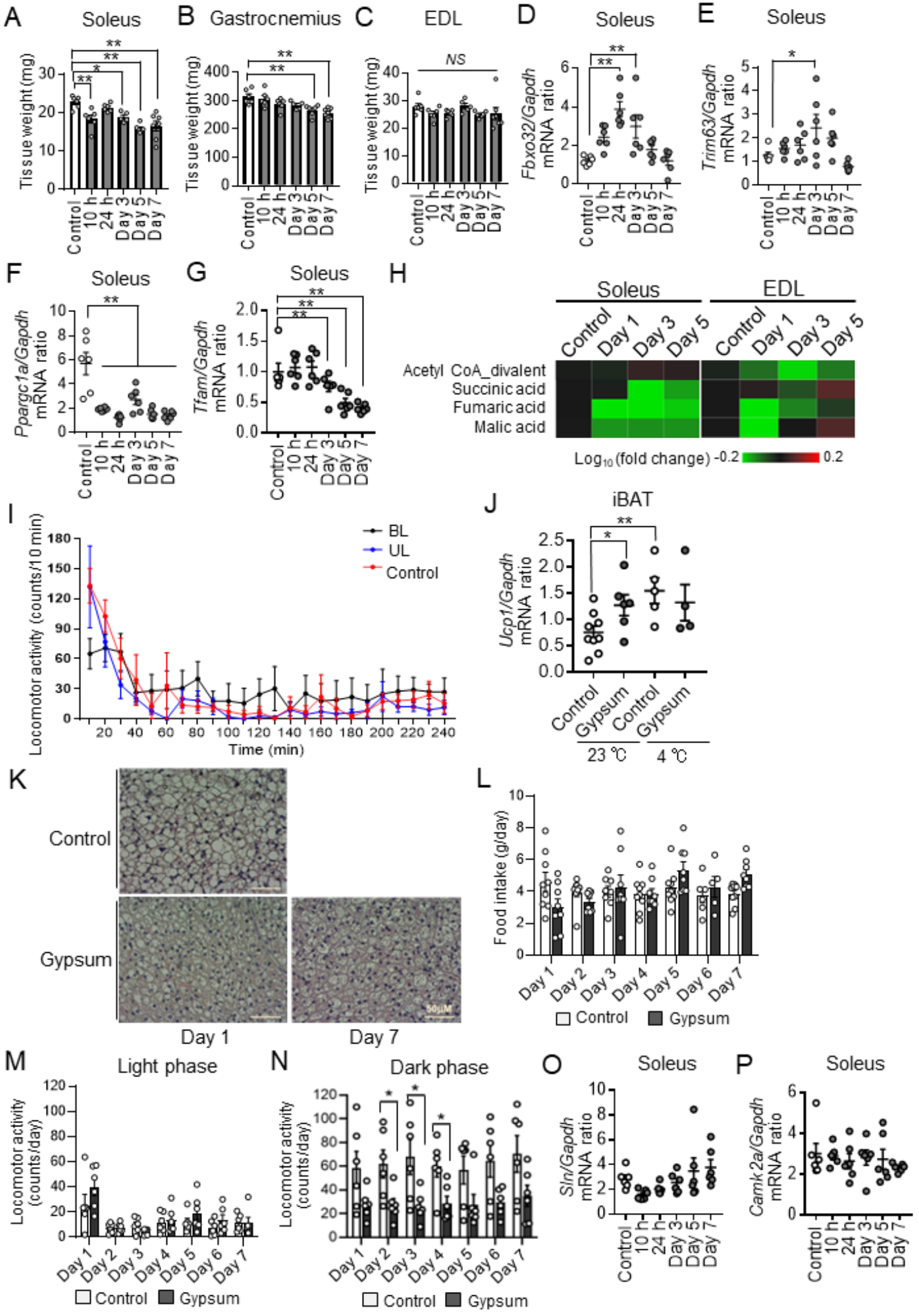

Figure 1_figure supplement 2

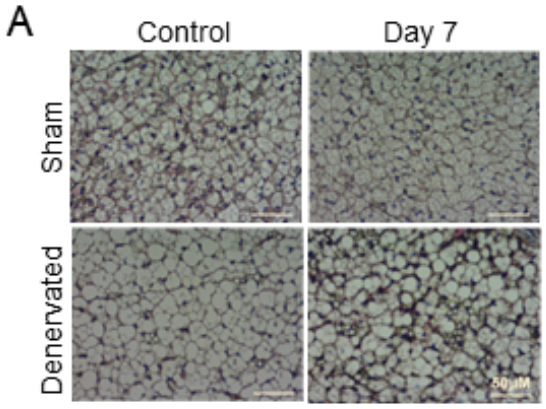

Figure 2_figure supplement 1

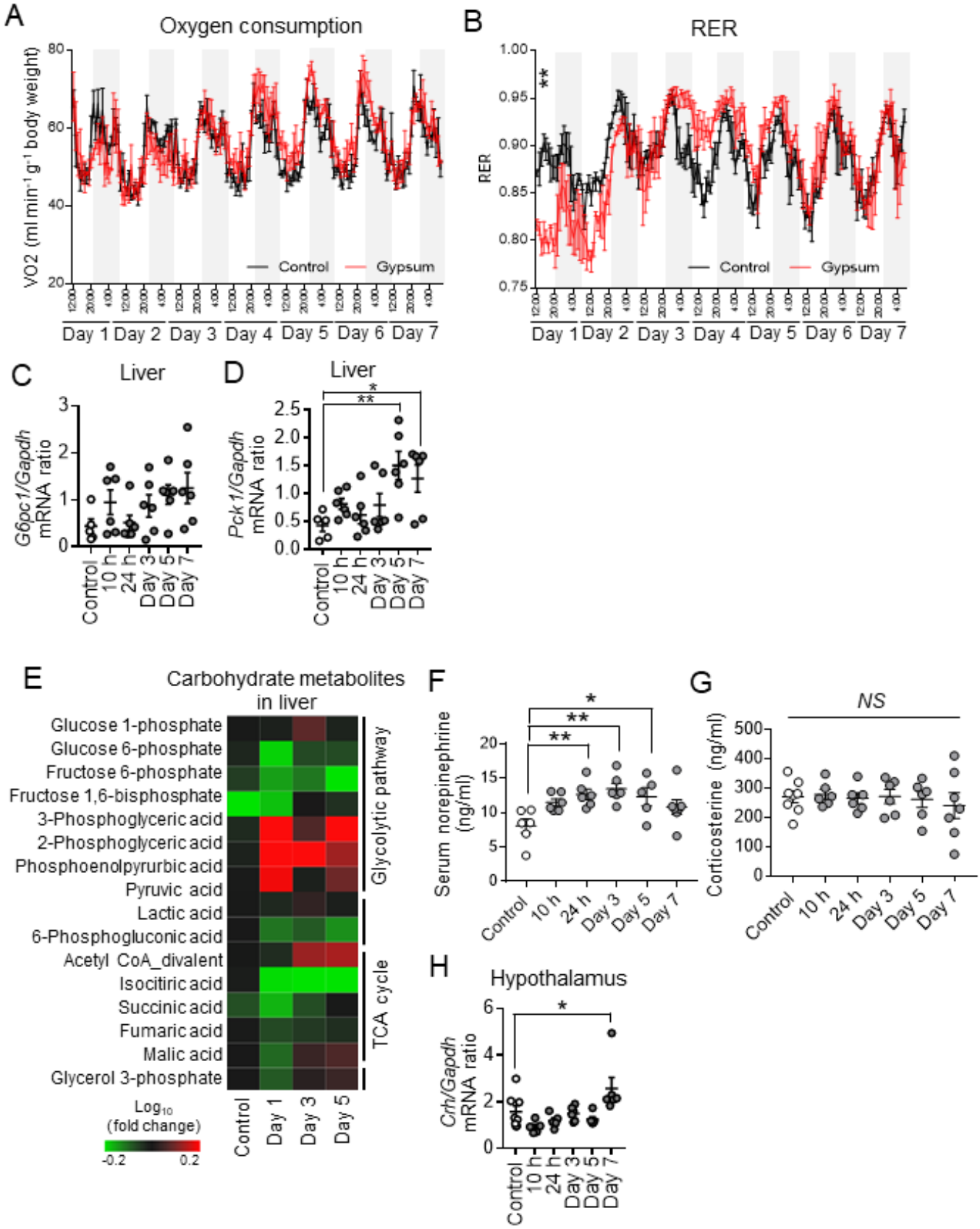

Figure 3_figure supplement 1

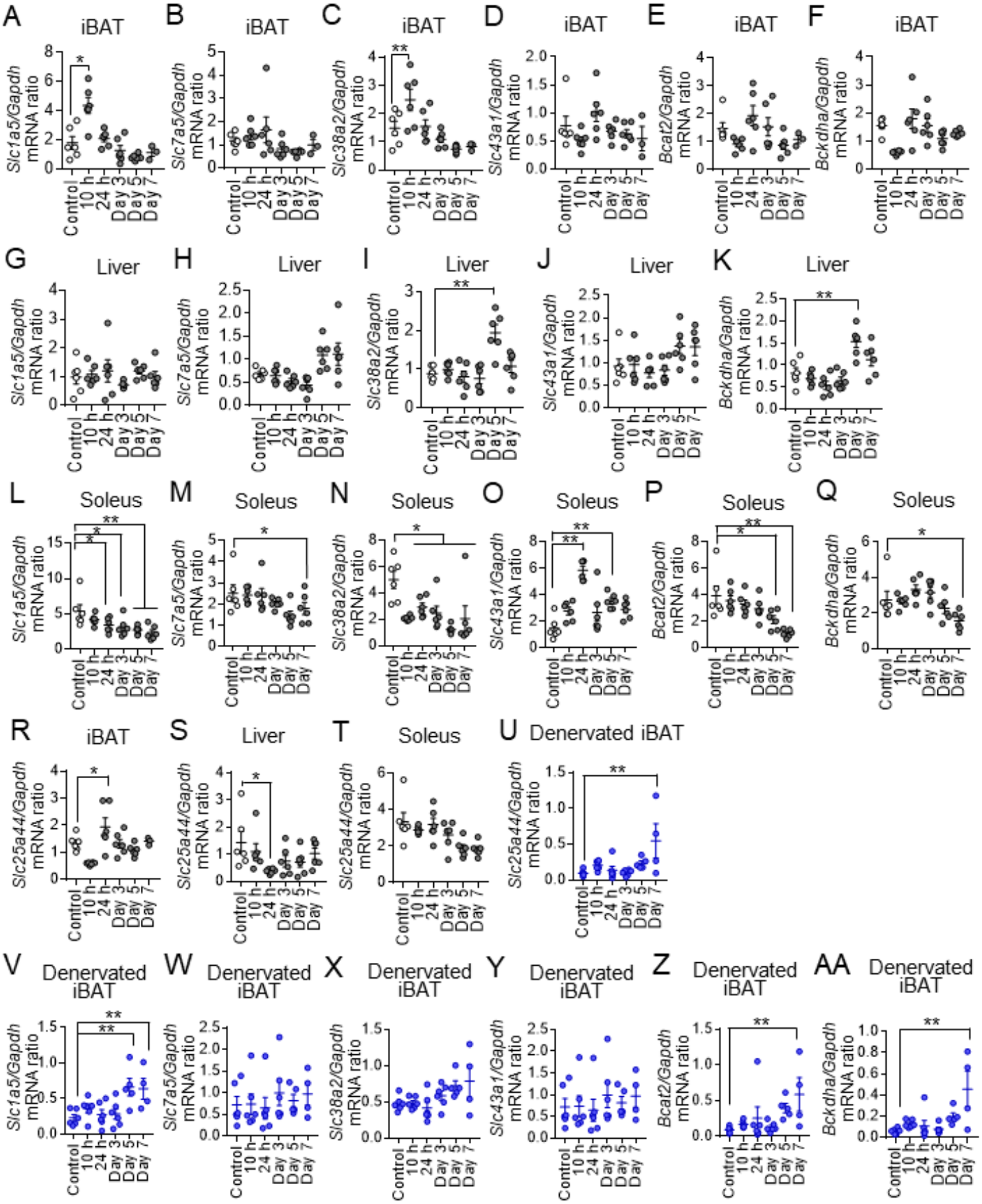

Figure 4_figure supplement 1

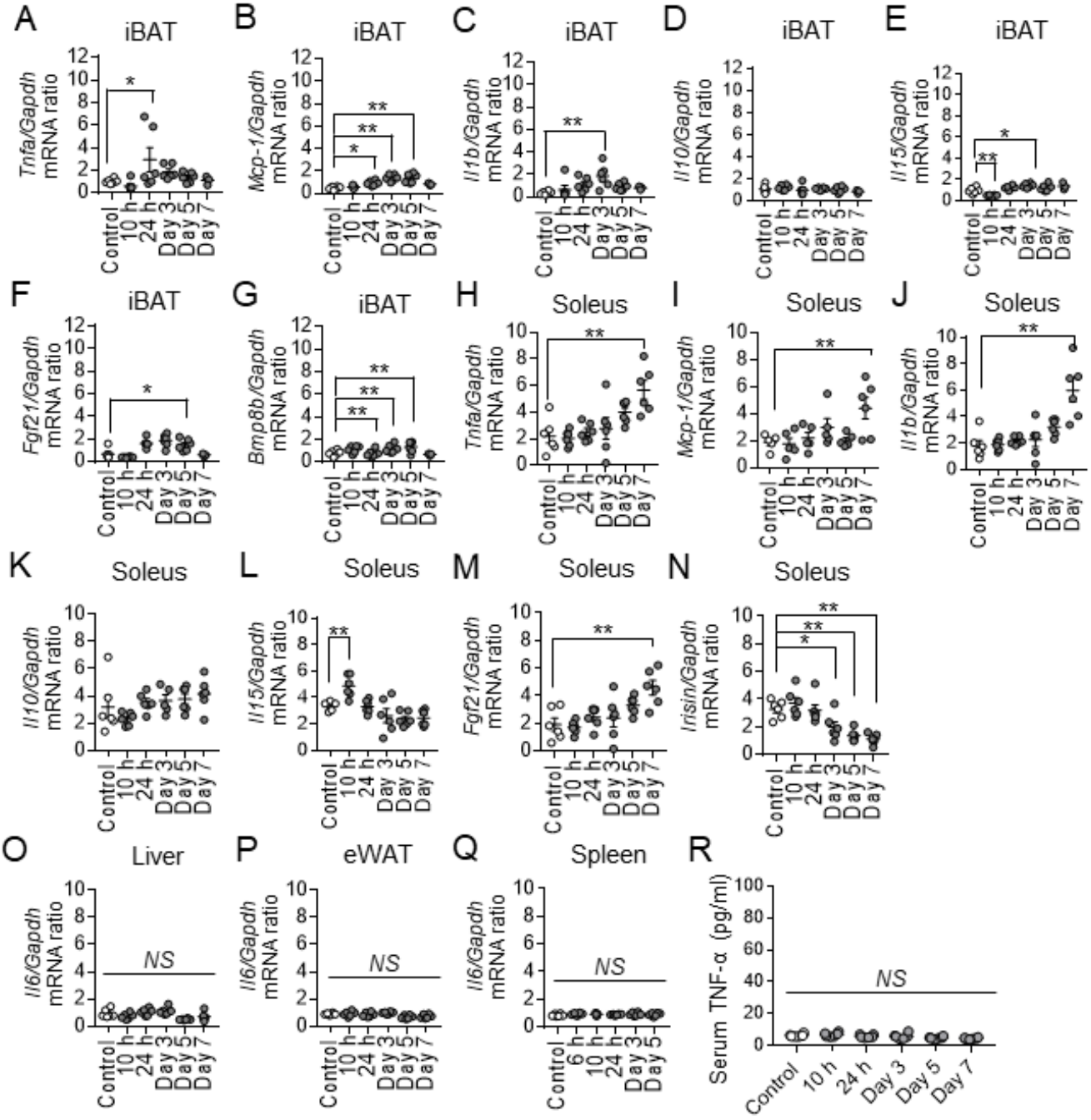

Figure 5_figure supplement 1

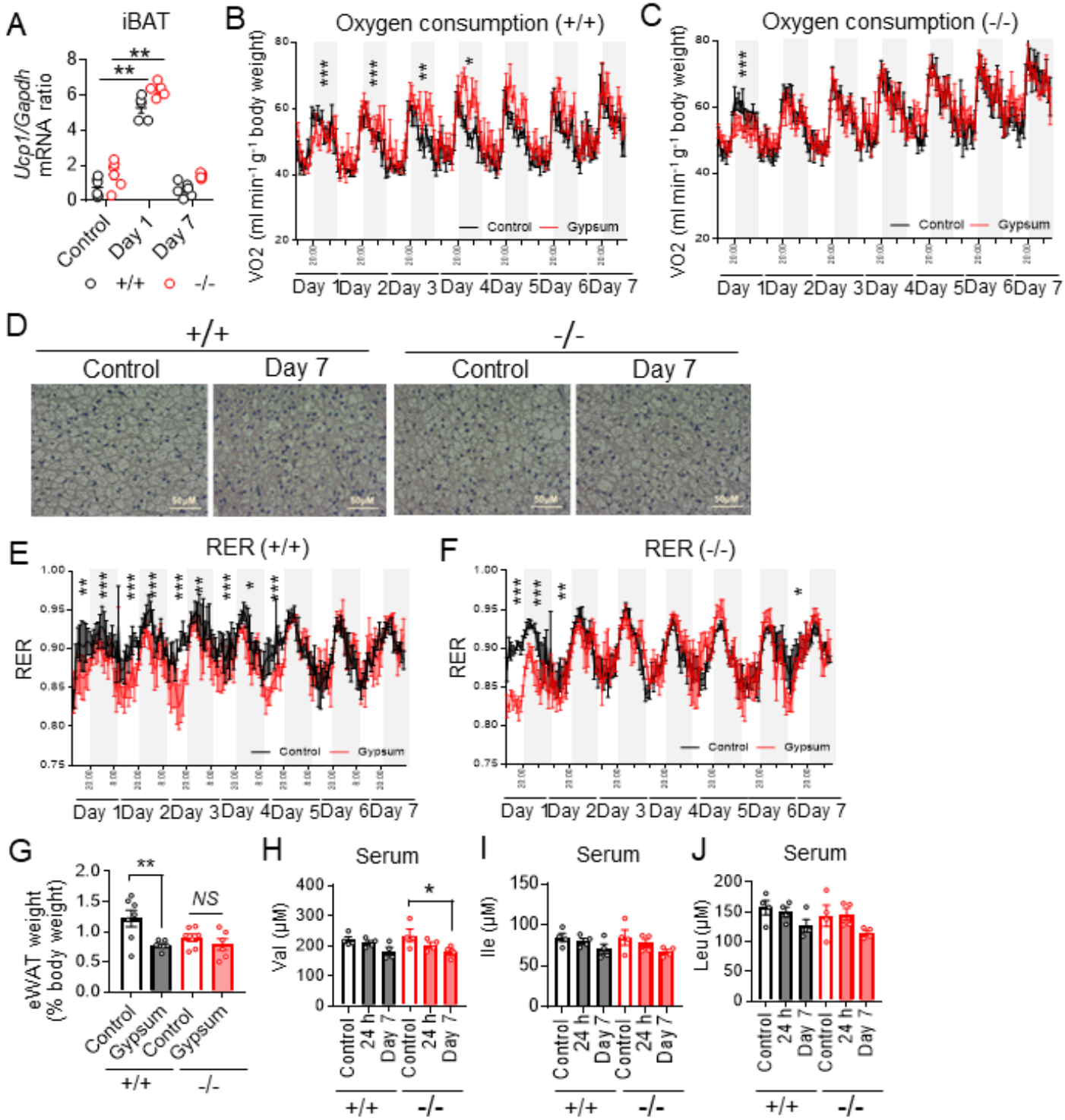

Figure 6_figure supplement 1

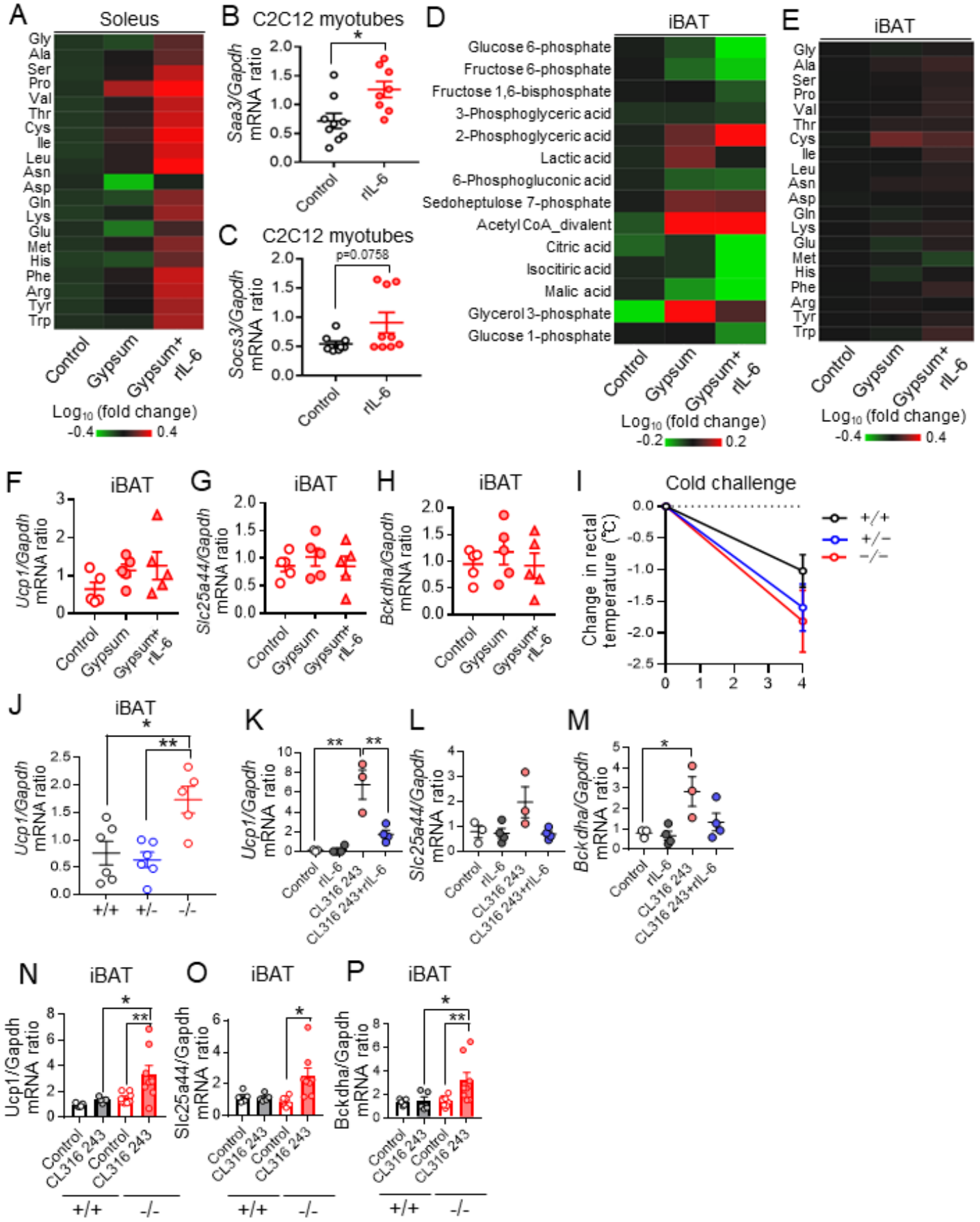
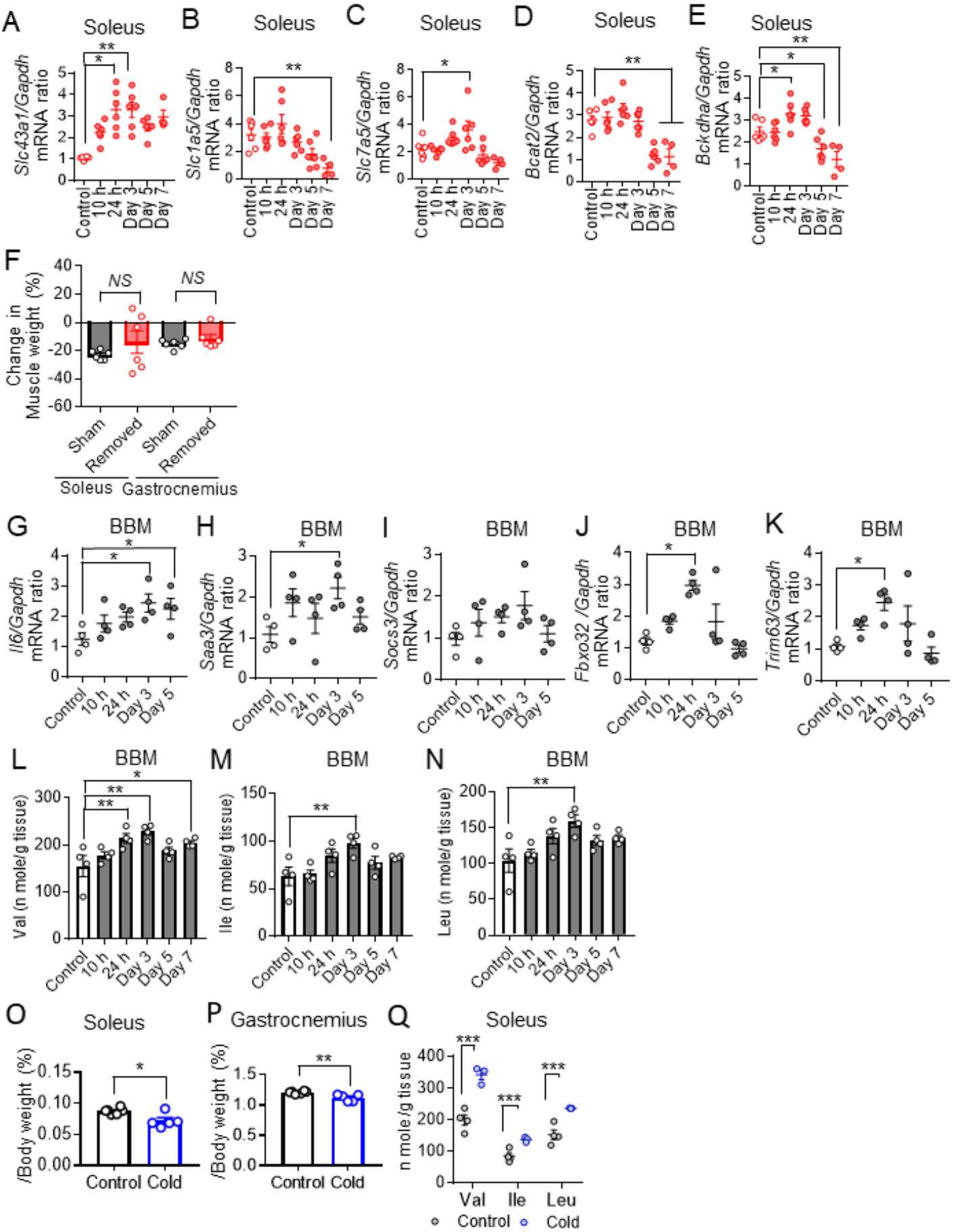
Figure 6_figure supplement 2